haematologica
Journal of The Ferrata Storti Foundation

Extracellular vesicles mediate the communication between multiple myeloma and bone marrow microenvironment in a NOTCH dependent way

by Domenica Giannandrea, Natalia Platonova, Michela Colombo, Mara Mazzola, Valentina Citro, Raffaella Adami, Filippo Maltoni, Silvia Ancona, Vincenza Dolo, Ilaria Giusti, Andrea Basile, Anna Pistocchi, Laura Cantone, Valentina Bollati , Lavinia Casati, Elisabetta Calzavara, Mauro Turrini, Elena Lesma, and Raffaella Chiaramonte

Received: August 11, 2021.
Accepted: March 2, 2022.

Citation: Domenica Giannandrea, Natalia Platonova, Michela Colombo, Mara Mazzola, Valentina Citro, Raffaella Adami, Filippo Maltoni, Silvia Ancona, Vincenza Dolo, Ilaria Giusti, Andrea Basile, Anna Pistocchi, Laura Cantone, Valentina Bollati , Lavinia Casati, Elisabetta Calzavara, Mauro Turrini, Elena Lesma, and Raffaella Chiaramonte. Extracellular vesicles mediate the communication between multiple myeloma and bone marrow microenvironment in a NOTCH dependent way. Haematologica. 2022 Mar 10. doi: 10.3324/haematol.2021.279716. [Epub ahead of print]

Extracellular vesicles mediate the communication between multiple myeloma and bone marrow microenvironment in a NOTCH dependent way

Domenica Giannandrea[1], Natalia Platonova[1], Michela Colombo[1], Mara Mazzola[2], Valentina Citro[1], Raffaella Adami[1], Filippo Maltoni[1], Silvia Ancona[1], Vincenza Dolo[3], Ilaria Giusti[3], Andrea Basile[4], Anna Pistocchi[2], Laura Cantone[5], Valentina Bollati[5], Lavinia Casati[1], Elisabetta Calzavara[6], Mauro Turrini[6], Elena Lesma[1], Raffaella Chiaramonte[1]

1 Department of Health Sciences, Università degli Studi di Milano

2 Department of Medical Biotechnology and Translational Medicine, Università degli Studi di Milano

3 Department of Life, Health and Environment Sciences, Università degli Studi dell'Aquila

4 Department of Oncology and Hemato-oncology, Università degli Studi di Milano

5 Department of Clinical Sciences and Community Health, Università degli Studi di Milano

6 Division of Hematology, Valduce Hospital, Como, Italy

Correspondence:
Raffaella Chiaramonte,
Department of Health Sciences
Università degli Studi di Milano
via A. Di Rudinì, 8, Milan I-20142, Italy
e-mail: raffaella.chiaramonte@unimi.it

Acknowledgments

This study was supported by grants from Associazione Italiana Ricerca sul Cancro, Investigator grant to RC (20614), My First Grant to AP (18714); Fondazione Italiana per la Ricerca sul Cancro to MC (post-doctoral fellowship 18013); Università degli Studi di Milano to RC (Linea 2B-2017 - Dept. Health Sciences), to NP (post-doctoral fellowship type A) and DG (PhD fellowship in Experimental Medicine).

Conflict of interest statement

The authors declare no conflicts of interest.

Contributions

DG, NP, MC: Experiment design and performance, acquisition of data, drafting the manuscript; MM, VC, RA, FM, SA, EL: experiment performance, acquisition of data; VD and IG: TEM morphologic analysis; MC, MM, AP: performance of in vivo zebrafish experiment; DG, LCan and VB: NTA analysis; MT, EC: collection of patients' sample and clinical information and patients' sample first processing; DG, MT, AB, LCas: Statistical analysis; DG, MT, AB, AP, EL, VB, LCas: manuscript revision; LCas: acquisition of data; RC, DG, AB, MT: interpretation of data; RC: Experiment design and supervision, interpretation of data and statistical analysis, drafting, writing and critical revision of the manuscript.

Data sharing statement: for any question, please contact the corresponding author.

Keywords: multiple myeloma, NOTCH, extracellular vesicles, osteoclastogenesis, angiogenesis.

Word count

Abstract: 248

Main text: 4109 words

Abstract

Multiple myeloma (MM) is an incurable hematologic neoplasm, whose poor prognosis is deeply affected by the propensity of tumor cells to localize in the bone marrow (BM) and induce the pro-tumorigenic activity of normal BM cells, leading to events associated with tumor progression, including tumor angiogenesis, osteoclastogenesis, and the spread of osteolytic bone lesions.

The interplay between MM cells and the BM niche does not rely only on direct cell-cell interaction, but a crucial role is also played by MM-derived extracellular vesicles (MM-EV). Here, we demonstrated that the oncogenic NOTCH receptors are part of MM-EV cargo and play a key role in EV pro-tumorigenic ability. We used *in vitro* and *in vivo* models to investigate the role of EV-derived NOTCH2 in stimulating the pro-tumorigenic behaviour of endothelial cells and osteoclast progenitors. Importantly, MM-EV can transfer NOTCH2 between distant cells and increase NOTCH signaling in target cells. MM-EV stimulation increases endothelial cell angiogenic ability and osteoclast differentiation in a NOTCH2 dependent way. Indeed, interfering with NOTCH2 expression in MM cells may decrease the amount of NOTCH2 also in MM-EV and affect their angiogenic and osteoclastogenic potential. Finally, we demonstrated that the pharmacologic blockage of NOTCH activation by γ-Secretase inhibitors may hamper the biological effect of EV derived by MM cell lines and by the BM of MM patients.

These results provide the first evidence that targeting the NOTCH pathway may be a valid therapeutic strategy to hamper the pro-tumorigenic role of EV in MM as well as other tumors.

Introduction

Multiple myeloma (MM) is a clonal plasma cell neoplasm representing alone 13% of all hematological malignancies [1]. Despite the development of new therapies, MM still remains incurable [2], mainly due to MM cell ability to shape the bone marrow (BM) niche sustaining tumor progression. Upon the localization in the BM, MM cells establish anomalous signaling loops with the neighboring cells and "educate" BM-residing non-tumor cells to support different steps of MM progression, including tumor cell growth, survival, angiogenesis, and bone osteolysis [3].

In this complex picture, extracellular vesicles (EV) are new key players recently come to light. EV include a heterogeneous group of cell-derived membranous structures classified into two main subtypes according to their origin. Exosomes, the smaller ones, originate from the endosomal system, while the larger vesicles are shed from the plasma cell membrane. Due to the difficulty to distinguish these subtypes based on their origin, a recent position statement of the International Society for Extracellular Vesicles has suggested a distinction based on their size: i.e. small EV < 200nm and large EV > 200nm [4].

EV are key mediators in the communication between tumor and stroma due to their ability to transport proteins and RNAs [5]. Circulating EV from MM patients display characteristic size distribution and concentration [6, 7], and their miRNA cargo is prognostic in MM [8-10]. Recent evidence indicates that MM cell-derived EV (MM-EV) modulate the BM niche, promoting angiogenesis, immunosuppression [11], and bone disease [12]. Additionally, several features of MM-EV may contribute to MM dissemination at distant sites, thereby favoring skeletal metastasis formation, progression and bone disease [13].

This work elucidates how MM cells exploit the aberrantly expressed NOTCH2 oncogene to shape the BM niche *via* MM-EV, specifically focusing on tumor angiogenesis and osteoclastogenesis.

NOTCH is a family of transmembrane receptors (NOTCH1-4) activated by the interaction with five different membrane-bound ligands (JAGGED1-2 and DLL1-3-4) present on the adjacent cells. The consequence of this interaction is the cleavage by γ–Secretase, which releases the active form of NOTCH (NOTCH-IC) from the cell membrane and allows its translocation to the nucleus and the activation of the CSL transcription factors [14].

NOTCH deregulation in MM cells is due to the aberrant expression of NOTCH receptors and/or ligands [15]. High levels of NOTCH pathway activity are associated with increased myeloma cell infiltration in BM biopsies of MM patients [16]. Other studies suggest that MM cell skeletal infiltration may be due to events promoted by NOTCH, including MM cell recruitment at the BM [17], mitogenic or anti-apoptotic effect [17-19], or MM stem cell self-renewal [20]. Additionally, MM infiltration of BM niche is also associated with the activation of NOTCH signaling in the tumor niche, which promotes angiogenesis [16, 21], osteoclastogenesis [22-24], and bone marrow stromal cell (BMSC) release of cytokines involved in these events (IL-6, VEGF, IGF-1, SDF-1, RANKL, etc.) [16, 18, 19, 25].

Up to now, the increased activation of NOTCH signaling in the tumor microenvironment has been attributed to the presence of high levels of MM cell-derived-JAGGED ligands. Here, we demonstrate that MM cells may trigger tumor angiogenesis and osteoclastogenesis by transferring NOTCH2 receptor *via* EV. Moreover, we provide evidence that targeting the NOTCH pathway may represent a suitable strategy to hamper the MM-EV mediated pathological communication with the BM niche.

Methods

Extracellular vesicles isolation from HMCL and MM patients' BM aspirates

EV were obtained from supernatants of RPMI8226 and OPM2 cells cultured for 48 h in RPMI1640 medium depleted of FBS-derived bovine EV or from the plasma obtained by BM aspirates of monoclonal gammopathy of undetermined significance (MGUS) (MGUS-BM-EV) and MM patients (MM-BM-EV). The Institutional Review Board of Insubria Italy approved the design of this study (approval n. 1 on 27th February 2018). Written informed consent was obtained in accordance with the Declaration of Helsinki. Clinical information of patients is reported in table S1.

EV pellets were resuspended in the appropriate buffer/medium for subsequent studies. Further details are reported in Supplemental experimental procedures.

Production of viral supernatants and NOTCH2 knockdown

Viral supernatants were generated by calcium phosphate-DNA transfection of HEK293T cells with the Dharmacon Trans-lentiviral packaging kit containing pTRIPZ vector carrying a doxycycline-inducible system (Tet-on) expressing shRNAs against NOTCH2, or the corresponding scrambled shRNA (Horizon Discovery, United Kingdom). A pilot experiment on HEK293T cells was carried out by transient transfection of 4 shRNAs for NOTCH2 to select the more effective NOTCH2 shRNA (Cat.ID RHS5087-EG4853 - mature antisense sequence: ATGTCACAAGAGACATTGG). Lentiviral supernatants were used to infect and generate stable clones of RPMI8226 and OPM2 cells. shRNA expression was induced by treatment with 1µg/ml Doxycycline (Sigma Aldrich, Italy).

In vivo experiments

In vivo experiments were carried out on transgenic zebrafish (*Danio rerio*) embryos obtained by crossing *Tg(T2KTp1bglob:hmgb1-mCherry)* with *Tg(fli1a:EGFP)* obtained from the Wilson lab, University College London, United Kingdom. Zebrafish embryos were raised and maintained under standard conditions and national guidelines (Italian decree 4th March 2014, n.26). All experiments have been conducted within 5 days post fertilization (dpf). EV were injected into the duct of Cuvier of embryos at 48 h post fertilization (hpf) with a manual microinjector (Eppendorf, Germany) using glass microinjection needles.

Further details on the above procedures and information concerning cell cultures, transmission electron microscopy, *in vitro* uptake, western blot, EV-derived NOTCH2 tracking system, viral particle production, luciferase reporter assay, *in vivo* experiments, osteoclastogenesis and angiogenesis assays, *ex vivo* experiments and statistical analyses are reported in Supplemental experimental procedures.

Results

Multiple myeloma-derived extracellular vesicles are uptaken by bone marrow cell populations

EV produced by two different human MM cell lines (HMCL), RPMI8226 and OPM2, were isolated by ultracentrifugation and fully characterized. Particle size distribution assessed by nanoparticle tracking analysis (NTA) revealed that the EV populations produced by the two HMCL were characterized by the presence of both small (30-200 nm) and large (200-1000 nm) vesicles (Fig. 1A). The shape and integrity of MM-EV have been assessed by transmission electronic microscopy (TEM), showing the presence of whole, undamaged small and large EV (Fig. 1B).

We assessed the ability of MM-EV to transfer their content to two key BM cell populations crucial in supporting MM progression, osteoclasts (OCL) and endothelial cells (EC). The uptake was assessed in a quantitative (Fig. 2A and 2B) and qualitative way (Fig. 2C). EV isolated by a 48 h culture of RPMI8226 cells were stained with the fluorescent lipophilic dye CM-DIL and put in contact with a monolayer of OCL progenitors (Raw264.7 cells) and EC (primary human pulmonary arterial cells – HPAEC) for 4 h at 37°C. The negative control was maintained at 4°C to inhibit the uptake. In Fig.2A-B, MM-EV uptake was quantified through flow cytometry by measuring the CM-DIL fluorescent signal in receiving cells. The dot plot analysis clearly shows that the two different cell types uptake MM-EV with a similar efficiency. The graph in Fig.S1 summarizes the mean values and statistical analysis of flow cytometry detection. These results were confirmed by fluorescence microscopy analysis. Stack projection images (Fig. 2C) and z-stack videos (supplementary videos) show the presence of high levels of fluorescent signal in Raw264.7 (supplemental video 1) and HPAEC cells (supplemental video 2) treated with MM-EV at 37°C, indicating that MM-EV may be internalized by these cells. As expected, internalization is blocked when cells are kept at 4°C, suggesting that an active process is involved.

Multiple myeloma-derived extracellular vesicles carry NOTCH2

Due to the important role of NOTCH in the interplay between MM and the BM microenvironment, we wondered if MM-EV contribute to NOTCH activation in BM cells by carrying NOTCH receptors and, in particular the overexpressed receptor NOTCH2 [26], as part of their cargo. By western blot analysis, we compared NOTCH2 expression in protein extracts from 7 HMCL, namely AMO1, JJN3, H929, RPMI8226, LP1, KMS12, OPM2, and EV isolated from conditioned media (CM). Fig. 3A shows that MM-EV are able to carry NOTCH2, those relative amount reflects that expressed in the different protein extracts of the HMCL.

The analysis of the different forms of NOTCH2 indicated that MM-EV could carry not only the transmembrane NOTCH2 (NOTCH2-TM) but also the full-length uncleaved NOTCH2 (NOTCH2-FL). Since the cleavage operated by γ-Secretase on the intracellular portion of NOTCH takes place inside the endocytic bodies [27] and exosomes arise from late endosomes [28], we investigated whether the active cleaved intracellular NOTCH2-IC may be included in MM-EV cargo by using a specific antibody. Results in Fig. 3A indicate that MM-EV cargo also carries NOTCH2-IC. Fig. S2 shows that also NOTCH1 is widely represented in MM-EV, while the presence of other two isoforms in MM-EV is less noticeable.
To assess which EV fraction expresses NOTCH2, we performed a western blot analysis on large and small vesicles collected from the HMCL CM by sequential ultracentrifugation at 20,000 g and 110,000 g (110 K). We found that NOTCH2-TM and NOTCH2-IC were present both in large and small vesicles (Fig.3B). Interestingly, NOTCH2-IC level was increased in 110K MM-EV fraction.

EV allow distant cells to communicate between each other, thus modifying their behaviour. To demonstrate that NOTCH2 may be involved in these processes and can be transferred to distant cells *via* EV, we developed a model system of HEK293 donor and receiving cells (Fig.3C). The first were forced to constitutively express NOTCH2 tagged with HA at the C-terminus (NOTCH2-HA) [29] to distinguish it from the endogenous NOTCH2. In addition, the position of the HA tag at the C-terminus of NOTCH2 enabled us to detect NOTCH2-FL, the NOTCH2-TM portion of the heterodimeric NOTCH2 form, matured in the trans-Golgi network upon the cleavage by a furin-like convertase [30], and the mature NOTCH2-IC, due to homotypic activation mediated by ADAM10 and the γ-secretase [29]. EV-donor cells were added to the colture medium of receiving HEK293 cells. Fig.3C shows a western blot analysis performed with an anti-HA antibody, confirming the presence of the HA-signal in donor cells carrying NOTCH2-HA, isolated EV, and receiving cells. This demonstrate that EV can transfer NOTCH2 between distant cells. In this model system, the EV cargo include NOTCH2-TM and NOTCH2-FL, while both donor and receiving cells show also the presence of NOTCH2-IC. The absence of NOTCH2-IC in HEK293-derived EV might be due to a lower level of NOTCH activation in HEK293 cells in comparison to HMCL.

Multiple myeloma-derived extracellular vesicles activate NOTCH signaling in receiving cells

To address if the variation of NOTCH2 levels in MM cells may affect MM-EV mediated communication, we studied the effect of NOTCH2 silencing in RPMI8226 and OPM2 cells. These cells were transduced with the pTRIPZ lentiviral vector conditionally expressing shRNAs for NOTCH2 ($HMCL^{N2KD}$) or the scrambled sequence ($HMCL^{SCR}$) and single cell clones were isolated. Fig. 4A confirms that RPMI8226 and OPM2 cells are knocked down (KD) for NOTCH2 and clearly shows that also the produced MM-EV displayed a reduced level of NOTCH2. Also NOTCH2-IC decreased in OPM2 cells with a corresponding decrease in the shed EV, while NOTCH2-IC decrease in EV release from RPMI8226 was less evident (Fig.S4). Through alignment search tool BlastN (USA National Center for Biotechnology Information) we excluded regions of local similarities between the used shRNA and the sequences of other NOTCH receptors and ligands (E

values range between 1 and 15). The high sequence homology between the four NOTCH receptors prompted us to analyze by western blot the expression of the other NOTCH receptor isoforms. Fig. 5S shows that NOTCH2 KD did not affect the expression of NOTCH1, 3 and 4 in protein extracts from cells and MM-EV. The outcome of NOTCH2 KD on EV size and concentration evaluated by NTA showed no significant effect on MM-EV size and concentration (Fig. 4B).

To assess if the NOTCH2 protein carried by MM-EV is functionally active and is able to trigger NOTCH signaling in receiving cells, we tested the effect of EV isolated from $HMCL^{N2KD}$ ($MM\text{-}EV^{N2KD}$) or $HMCL^{SCR}$ ($MM\text{-}EV^{SCR}$) through a NOTCH responsive luciferase reporter assay. This assay was carried out in the HeLa cell line, which is highly transfectable and characterized by a low level of NOTCH signaling activation (not shown). Fig. 4C shows that $MM\text{-}EV^{SCR}$ can activate the NOTCH signaling pathway in the receiving HeLa cells, while this ability is significantly reduced for $MM\text{-}EV^{N2KD}$.

The ability of MM-EV to activate NOTCH signaling was also validated in an *in vivo* NOTCH reporter zebrafish embryo obtained by crossing *Tg(T2KTp1bglob:hmgb1-mCherry)* with *Tg(fli1a:EGFP)* that carry EGFP+ endothelial cells (green) and express the mCherry protein (red) under the control of a NOTCH-responsive element. EV isolated from RPMI8226 cells were injected in the duct of Cuvier of 48 hpf transgenic zebrafish embryos. Images were acquired 4 h post-injection. Fig. 4D shows $MM\text{-}EV^{SCR}$ mediated NOTCH activation in the intersegmental vessels (Se), caudal artery (CA), and in the area of the caudal hematopoietic tissue (CHT), while $MM\text{-}EV^{N2KD}$ induces a barely visible stimulation.

NOTCH2 carried by multiple myeloma-derived extracellular vesicles contributes to the education of bone marrow cell populations

We and other groups previously reported that MM cells affect the surrounding BM microenvironment inducing osteoclastogenesis [22-24] and tumor angiogenesis [16, 21] in a NOTCH-dependent way. Moreover, recent evidence indicates that MM-EV stimulate osteoclastogenesis [13, 31-33], angiogenesis and carry pro-angiogenic proteins [11, 34]. Therefore, we verified the osteoclastogenic potential of $MM\text{-}EV^{SCR}$ and $MM\text{-}EV^{N2KD}$ by treating the monocyte cell line Raw264.7 in the presence of the osteoclastogenic chemokine RANKL (30 ng/ml). We used MM-EV released by the RPMI8226 cell line due to the ability of these cells to induce osteoclastogenesis, differently from OPM2 cells [22]. After 7 days of treatment with MM-EV, OCL count showed that $MM\text{-}EV^{SCR}$ induced Raw264.7 cell differentiation, while $MM\text{-}EV^{N2KD}$ lost this ability (Fig. 5A).

We assessed $MM\text{-}EV^{N2KD}$ angiogenic potential using a tube formation assay with HPAEC seeded on a Matrigel layer. Results in Fig.5B show that $MM\text{-}EV^{SCR}$ promotes tube organization of HPAEC, while treatment with $MM\text{-}EV^{N2KD}$ reduces this effect. In conclusion, this specific RNA interference approach unequivocally demonstrated that NOTCH2 KD affects the MM-EV mediated osteoclastogenesis and angiogenesis.

Targeting NOTCH signaling blocks the pathological communication mediated by multiple myeloma-derived extracellular vesicles

To provide a higher translational potential to our findings we exploited the strategy illustrated in Fig.6A. We used γ-secretase inhibitors (50 µg/ml DAPT), used in research works and clinics to inhibit pan-Notch signaling [15] to block NOTCH activation in EC and OCL induced by MM-EV. Fig.6B and C clearly show that MM-EV induce angiogenesis and osteoclastogenesis in a NOTCH-dependent way. In consideration of the well known osteoclastogenic and angiogenic roles of NOTCH signaling [16, 21-24], we planned our experiments to distinguish the effect of the endogenous and vesicular NOTCH. Indeed, if we compare the effect of DAPT on osteoclastogenesis (fig.6B) in the absence of EV and suboptimal concentration of RANKL, we can see that it abrogates OCL differentiation with a non-statistically significant decrease, while DAPT abrogates much higher levels of osteoclastogenesis induced by MM-EV (+250%) in a statistically significant way, indicating that the greater effect of MM-EV is NOTCH dependent.

The effect of DAPT on MM-EV induced angiogenesis was analogous. The high increase of HPAEC tube organization upon the administration of MM-EV from RPMI8226 and OPM2 cells was completely abrogated by DAPT, showing a statistically significant reduction in areas and nodes (ranging from 29,5% to 51,3%). This effect was clearly higher than the slight inhibitory trend observed on basal angiogenesis upon DAPT administration (Fig. 6C). We also ruled out that the obtained results could be due to the toxic effect of DAPT on OCL and EC (Fig. S6).

Overall, these results confirm that the studied biological effects of EV are NOTCH mediated and can be blocked by treatment with γ-Secretase inhibitors.

Finally, to strengthen the translational potential of our *in vitro* findings, we reasoned that the BM of MM patients does not contain only MM-derived EV, but EV derived from the whole MM-educated BM cell populations. Therefore to confirm the NOTCH-dependent role of EV in the pathological communication occurring in the BM of MM patients, we have got advantage of EV from BM aspirates of patients with the benign MGUS (MGUS-BM-EV) or MM (MM-BM-EV) (Table S1), which may recapitulate the complexity of the BM microenvironment. We compared the angiogenic potential of HPAEC untreated or treated with MGUS-BM-EV or MM-BM-EV. Fig. 6D shows that MM-BM-EV boost the angiogenic potential of HPAEC while MGUS-BM-EV showed a non-statistically significant increasing trend. Importantly, the inhibitory effect of DAPT is statistically significant when added to HPAEC treated with MM-BM-EV. These results confirm the increasing angiogenic potential of EV released in the BM during MM progression, the role played by NOTCH delivered via MM-BM-EV and strengthen the potential of a NOTCH-directed therapeutic approach to block the support of MM microenvironment to the disease progression.

Discussion

The pathological interplay between malignant cells and the surrounding non-tumoral BM cells promotes neoplastic cell growth and survival as well as key events of tumor progression including bone disease and angiogenesis. These lines of evidence suggest that an effective therapeutic approach should not be focused merely on the MM cells, but it should target their interaction with the surrounding BM niche.

Recently, EV have been reported as critical players in the communication between MM cells and the nearby BM cells and leading to MM progression. Indeed, MM-EV promote different events associated with MM progression, including angiogenesis [11, 13, 34, 35] and osteoclastogenesis [13, 31-33].

Here, we contribute to elucidate the molecular mechanisms involved in MM-EV pathological communication with the BM microenvironment, strengthening the role of the EV pathological communication as a promising therapeutic target in MM.

The evidence that NOTCH signaling activation, mediated by MM cell heterotypic interaction with the surrounding BM cells, plays a key role in tumor angiogenesis [16, 21] and osteoclastogenesis [22-24] prompted us to investigate whether NOTCH signaling contributes to determine the impact of MM-EV on these processes.

Our analysis on a panel of HMCL and the respective shed EV indicate that NOTCH receptors were present in MM-EV cargo with high levels of NOTCH2 and slightly lower levels of NOTCH1, consistently with evidence from other cell types [36]. We focused on NOTCH2 receptor, widely expressed in MM cell lines and in primary MM cells, particularly from high-risk patients [18, 26]. In details, we found that MM-EV carried the mature heterodimeric form of NOTCH2 (since we detected the NOTCH2-TM portion), the immature NOTCH2-FL and the activated NOTCH2-IC, that upon delivering to target cells might directly activate the transcription of the NOTCH target genes without requiring the interaction with ligands and the activation by ADAM protease and γ-Secretase.

The expression of NOTCH receptors has been reported in exosomes [37] but also in microvesicles [38]. Thereby, we wondered which of the two subpopulations of EV hosted NOTCH2. We separated large and small vesicles and found the presence of NOTCH2-TM both in large and small particles, while NOTCH2-IC level was higher in 110K small EV fraction. Although it is not possible to distinguish exosome and microvesicles only on the basis of their dimension, we presume that small vesicles are enriched with exosomes respect to large vesicles. Therefore our results suggest the presence of NOTCH2-IC within exosomes consistently with its presence in the endosomal compartment from which exosomes take origin.

Before validating the hypothesis that vesicular NOTCH2 contributes to molecular and biological effects on relevant BM cell population as OCL and EC, we monitored if these cells uptake MM-EV, using respectively Raw264.7 and HPAEC cells. Flow cytometry detection showed a quick (4 h) uptake of MM-EV by the majority of cells in both models, confirmed by a Z-stack analysis in confocal microscopy.

Additionally, we unequivocally assessed that NOTCH signaling members could be transferred via EV from one cell to another using an experimental system model based on HEK293 cells forced to express NOTCH2 tagged with HA. This model system allowed us to assess that NOTCH2-HA could be released

within EV and be transferred to distant cells. In this system, we have confirmed that EV carried high levels of NOTCH2-TM form and NOTCH2-FL, even if at much lower level. On the contrary, although the NOTCH2-IC form was present in MM-EV shed by HMCL, we could not detect it in HEK293-derived EV, possibly due to a lower level of NOTCH2 activation in HEK293 cells in comparison to HMCL. Receiving cells clearly uptook the transmembrane form of NOTCH2-HA, but also showed a very faint band corresponding to NOTCH2-IC, consistently with a slight NOTCH2 activation after EV uptake. This result provided a first indication that EV carrying NOTCH2 may activate NOTCH signaling in receiving cells.

Using a selective RNA interference of NOTCH2 in RPMI8226 and OPM2 cells, we confirmed that NOTCH2 KD in HMCL impacted the levels of vescicular NOTCH2-TM, NOTCH2-FL and NOTCH2-IC, although the decrease of the activated form was evident only in OPM2 cells. On the contrary, NOTCH2 KD did not significantly affectMM-EV size and concentration.

To confirm that MM-EV might activate the oncogenic NOTCH signaling in receiving cells, we tested MM-EV^{SCR} or MM-EV^{N2KD} in *in vitro* and *in vivo* NOTCH reporter systems. The first *in vitro* cellular model transfected with a Nanoluc-based NOTCH reporter vector, indicated that MM-EV^{SCR} might activate a NOTCH-dependent gene reporter, while MM-EV^{N2KD} induced a significantly lower activation. This result was confirmed by a second reporter *in vivo* system recapitulating the complexity of a whole organism. The injection of MM-EV^{SCR} or MM-EV^{N2KD} in transgenic zebrafish embryo reporter for NOTCH not only confirmed the observed MM-EV mediated NOTCH signaling activation but also provided evidence of MM-EV ability to induce NOTCH signaling activation at distant sites through the circulation. Indeed, MM-EV injected in the duct of Cuvier may be transported through the circulation and activate NOTCH signaling in the caudal hematopoietic tissue which represents the main hematopoietic organ in zebrafish embryo, analogously to the human BM [39]. In contrast, NOTCH signaling activation mediated by MM-EV^{N2KD} was significantly lower. MM-EV effectiveness in inducing NOTCH signaling activation at distant sites in zebrafish embryos carried by the blood stream suggests that MM-EV could also play an important role in the metastatic process, as reported for pancreatic cancer [40]. For instance they may help preparing the pre-metastatic niche through the formation of new permeable vessels for the extravasation of tumor cells, and destructing of the bone matrix to make space for metastatic cells.

Taken as a whole, the *in vitro* and *in vivo* NOTCH reporter assays confirmed that NOTCH activity in target cells was due to NOTCH2 delivered by the injected MM-EV.

This evidence and the acknowledged effect of NOTCH signaling on OCL and EC, prompted us to verify if NOTCH2 delivery by MM-EV could affect the biology of these cells. Through the same specific RNA interference approach on two different HMCL, we provided an unequivocal demonstration that vesicular NOTCH2 participates in MM-induced OCL differentiation and angiogenesis, assessed by a tube-formation assay. The dependency of these processes on NOTCH signaling was clearly demonstrated by the fact that MM-EV^{N2KD} impact was significantly lower. The presence of other NOTCH receptors in MM-EV cargo, even if at a lower level, (i.e. NOTCH1) suggests that they may also provide a contribution.

In order to strengthen the translational potential of our results we used a dual approach: 1) the outcome of an anti-NOTCH therapeutic approach already tested in clinics was assessed *in vitro* and *ex vivo*; 2) *ex vivo* experiments were carried out with EV released in the BM of MM patients, taking into account that a systemic treatment is expected to affect the communication of MM-EV, as well as that of EV from all the BM cell populations. In the first case, we showed that γ-Secretase inhibitors (GSI), already used in clinics [15], greatly affected MM-EV ability to inhibit angiogenesis and osteoclastogenesis *in vitro*. Concerning the second point, EV collected from the BM of MM patients, but not MGUS patients, displayed a clear pro-angiogenic effect that could be hampered by GSI.

In conclusion, the RNA interfering approach specific for NOTCH2 on HMCL, complemented by a pan-NOTCH chemical inhibition on HMCL- and MM patients' BM-derived EV, provides a new important evidence of the effect of NOTCH signaling pathway on EV mediated pathological communication in myelomatous BM. The important inhibitory effect of GSI suggests that the form of the NOTCH2 oncogene which mostly contributes to MM-EV mediated education is NOTCH2-TM and not NOTCH-IC whose activity is GSI resistant. Although, the presence of NOTCH2-IC in MM-EV cargo is much intriguing since it may deliver an active oncogenic signal, we believe that vesicular NOTCH-IC might be more relevant in tumor that expresses the constitutively active form of NOTCH, such as T-cell acute lymphoblastic leukemia.

In conclusion, our results strengthen the rationale for therapeutic approaches directed to inhibit NOTCH activation mediated by MM-EV, suggesting that they have the potential of interfering with the pathological communication of the MM cells mediated by EV in the short and potentially in the long range and, thereby, they may influence the cross-talk with the surrounding microenvironment and the dissemination of the disease at distant skeletal sites.

Supplementary Information is available at Haematologica website.

References

1. Kyle RA, Rajkumar SV. Multiple myeloma. Blood. 2008;111(6):2962-2972.
2. Cowan AJ, Allen C, Barac A, et al. Global Burden of Multiple Myeloma: A Systematic Analysis for the Global Burden of Disease Study 2016. JAMA Oncol. 2018;4(9):1221-1227.
3. Manier S, Sacco A, Leleu X, Ghobrial IM,Roccaro AM. Bone marrow microenvironment in multiple myeloma progression. J Biomed Biotechnol. 2012;2012:157496.
4. Thery C, Witwer KW, Aikawa E, et al. Minimal information for studies of extracellular vesicles 2018 (MISEV2018): a position statement of the International Society for Extracellular Vesicles and update of the MISEV2014 guidelines. J Extracell Vesicles. 2018;7(1):1535750.
5. Webber J, Yeung V,Clayton A. Extracellular vesicles as modulators of the cancer microenvironment. Semin Cell Dev Biol. 2015;40:27-34.
6. Caivano A, Laurenzana I, De Luca L, et al. High serum levels of extracellular vesicles expressing malignancy-related markers are released in patients with various types of hematological neoplastic disorders. Tumour Biol. 2015;36(12):9739-9752.
7. Krishnan SR, Luk F, Brown RD, et al. Isolation of Human CD138(+) Microparticles from the Plasma of Patients with Multiple Myeloma. Neoplasia. 2016;18(1):25-32.
8. Manier S, Liu CJ, Avet-Loiseau H, et al. Prognostic role of circulating exosomal miRNAs in multiple myeloma. Blood. 2017;129(17):2429-2436.
9. Caivano A, La Rocca F, Simeon V, et al. MicroRNA-155 in serum-derived extracellular vesicles as a potential biomarker for hematologic malignancies - a short report. Cell Oncol (Dordr). 2017;40(1):97-103.
10. Rajeev Krishnan S, De Rubis G, Suen H, et al. A liquid biopsy to detect multidrug resistance and disease burden in multiple myeloma. Blood Cancer J. 2020;10(3):37.
11. Wang J, De Veirman K, Faict S, et al. Multiple myeloma exosomes establish a favourable bone marrow microenvironment with enhanced angiogenesis and immunosuppression. J Pathol. 2016;239(2):162-173.
12. Zhang L, Lei Q, Wang H, et al. Tumor-derived extracellular vesicles inhibit osteogenesis and exacerbate myeloma bone disease. Theranostics. 2019;9(1):196-209.
13. Colombo M, Giannandrea D, Lesma E, Basile A,Chiaramonte R. Extracellular Vesicles Enhance Multiple Myeloma Metastatic Dissemination. Int J Mol Sci. 2019;20(13):3236.
14. Colombo M, Mirandola L, Platonova N, et al. Notch-directed microenvironment reprogramming in myeloma: a single path to multiple outcomes. Leukemia. 2013;27(5):1009-1018.
15. Colombo M, Galletti S, Garavelli S, et al. Notch signaling deregulation in multiple myeloma: A rational molecular target. Oncotarget. 2015;6(29):26826-26840.

16. Palano MT, Giannandrea D, Platonova N, et al. Jagged Ligands Enhance the Pro-Angiogenic Activity of Multiple Myeloma Cells. Cancers (Basel). 2020;12(9):2600.
17. Mirandola L, Apicella L, Colombo M, et al. Anti-Notch treatment prevents multiple myeloma cells localization to the bone marrow via the chemokine system CXCR4/SDF-1. Leukemia. 2013;27(7):1558-1566.
18. Colombo M, Galletti S, Bulfamante G, et al. Multiple myeloma-derived Jagged ligands increases autocrine and paracrine interleukin-6 expression in bone marrow niche. Oncotarget. 2016;7(35):56013-56029.
19. Colombo M, Garavelli S, Mazzola M, et al. Multiple myeloma exploits Jagged1 and Jagged2 to promote intrinsic and bone marrow-dependent drug resistance. Haematologica. 2020;105(7):1925-1936.
20. Chiron D, Maiga S, Descamps G, et al. Critical role of the NOTCH ligand JAG2 in self-renewal of myeloma cells. Blood Cells Mol Dis. 2012;48(4):247-253.
21. Saltarella I, Frassanito MA, Lamanuzzi A, et al. Homotypic and Heterotypic Activation of the Notch Pathway in Multiple Myeloma-Enhanced Angiogenesis: A Novel Therapeutic Target? Neoplasia. 2019;21(1):93-105.
22. Colombo M, Thummler K, Mirandola L, et al. Notch signaling drives multiple myeloma induced osteoclastogenesis. Oncotarget. 2014;5(21):10393-10406.
23. Schwarzer R, Kaiser M, Acikgoez O, et al. Notch inhibition blocks multiple myeloma cell-induced osteoclast activation. Leukemia. 2008;22(12):2273-2277.
24. Schwarzer R, Nickel N, Godau J, et al. Notch pathway inhibition controls myeloma bone disease in the murine MOPC315.BM model. Blood Cancer J. 2014;4:e217.
25. Houde C, Li Y, Song L, et al. Overexpression of the NOTCH ligand JAG2 in malignant plasma cells from multiple myeloma patients and cell lines. Blood. 2004;104(12):3697-3704.
26. van Stralen E, van de Wetering M, Agnelli L, et al. Identification of primary MAFB target genes in multiple myeloma. Exp Hematol. 2009;37(1):78-86.
27. Chastagner P,Brou C. Tracking trafficking of Notch and its ligands in mammalian cells. Methods Mol Biol. 2014;1187:87-100.
28. Rajagopal C,Harikumar KB. The Origin and Functions of Exosomes in Cancer. Front Oncol. 2018;8:66.
29. Groot AJ, Habets R, Yahyanejad S, et al. Regulated proteolysis of NOTCH2 and NOTCH3 receptors by ADAM10 and presenilins. Mol Cell Biol. 2014;34(15):2822-2832.
30. Blaumueller CM, Qi H, Zagouras P, Artavanis-Tsakonas S. Intracellular cleavage of Notch leads to a heterodimeric receptor on the plasma membrane. Cell. 1997;90(2):281-291.

31. Raimondi L, De Luca A, Fontana S, et al. Multiple Myeloma-Derived Extracellular Vesicles Induce Osteoclastogenesis through the Activation of the XBP1/IRE1α Axis. Cancers (Basel). 2020;12(8):2167.
32. Raimondo S, Saieva L, Vicario E, et al. Multiple myeloma-derived exosomes are enriched of amphiregulin (AREG) and activate the epidermal growth factor pathway in the bone microenvironment leading to osteoclastogenesis. J Hematol Oncol. 2019;12(1):2.
33. Faict S, Muller J, De Veirman K, et al. Exosomes play a role in multiple myeloma bone disease and tumor development by targeting osteoclasts and osteoblasts. Blood Cancer J. 2018;8(11):105.
34. Umezu T, Tadokoro H, Azuma K, et al. Exosomal miR-135b shed from hypoxic multiple myeloma cells enhances angiogenesis by targeting factor-inhibiting HIF-1. Blood. 2014;124(25):3748-3757.
35. Liu Y, Zhu XJ, Zeng C, et al. Microvesicles secreted from human multiple myeloma cells promote angiogenesis. Acta Pharmacol Sin. 2014;35(2):230-238.
36. Wang Q,Lu Q. Plasma membrane-derived extracellular microvesicles mediate non-canonical intercellular NOTCH signaling. Nat Commun. 2017;8(1):709.
37. Patel B, Patel J, Cho JH, et al. Exosomes mediate the acquisition of the disease phenotypes by cells with normal genome in tuberous sclerosis complex. Oncogene. 2016;35(23):3027-3036.
38. Suwakulsiri W, Rai A, Xu R, et al. Proteomic profiling reveals key cancer progression modulators in shed microvesicles released from isogenic human primary and metastatic colorectal cancer cell lines. Biochim Biophys Acta Proteins Proteom. 2019;1867(12):140171.
39. Sacco A, Roccaro AM, Ma D, et al. Cancer Cell Dissemination and Homing to the Bone Marrow in a Zebrafish Model. Cancer Res. 2016;76(2):463-471.
40. Ogawa K, Lin Q, Li L, et al. Prometastatic secretome trafficking via exosomes initiates pancreatic cancer pulmonary metastasis. Cancer Lett. 2020;481:63-75.

Figure legends

Fig. 1: Characterization of MM cell-released EV. Extracellular vesicles (EV) from multiple myeloma cell lines (HMCL) RPMI8226 and OPM2 cells (MM-EV), were isolated by ultracentrifugation and analyzed by **A)** nanotracking particle analysis (NTA) and **B)** electron transmission microscopy (TEM). **A)** NTA analysis reveals the presence of small (30-200 nm) and large (200-1000 nm) vesicles. Size and concentration of EV were determined by NanoSight NS300 system (Malvern Panalytical Ltd, Malvern, UK). A camera level of 12 and five 30-s recordings were used for acquisition of each sample of 3 independent EV isolations and one representative image is shown. **B)** TEM analysis confirms the isolation of intact small and large vesicles.

Fig.2: MM-EV can be uptaken by osteoclasts and endothelial cells. **A-C)** Osteoclast (OCL) progenitors and endothelial cell (EC) uptake MM-EV from RPMI8226 cells. Raw264.7 cells and HPAEC have been treated with CM-DIL stained MM-EV or the negative control for 4 h at 37°C or 4°C. **A-B)** Representative flow cytometry dot-plots show the CM-DIL labeled RPMI8226-EV uptake by Raw264.7 cells (A) and HPAEC (B) by measuring CM-DIL positive cells in the PE channel. OPM2-EV provided similar results (not shown). Data are presented as mean values of three independent experiments **C)** Maximum intensity projection of CM-DIL positive RPMI8226-EV internalization in Raw264.7 cells and HPAEC after 4 h of incubation at 37°C and 4°C. Red fluorescence: RPMI8226-EV labeled with CM-DIL dye; green fluorescence: CFSE+labeled cells; blue fluorescence: nuclei with DAPI (63x magnification).

Fig.3: NOTCH receptors and ligands in EV. **A)** Western blot analysis for NOTCH2-FL (full length), NOTCH2-TM (transmembrane form), and NOTCH2-IC (active intracellular NOTCH2) expressed in 7 different HMCL and the respective produced EV. β-Actin and TSG101 have been used as loading controls for cells and vesicle protein extracts, respectively. To perform all the hybridizations, two western blots have been performed with cell and EV extracts loaded with the identical amount of proteins. **B)** A western blot analysis show the expression of NOTCH2-TM and NOTCH2-IC in EV populations of different sizes. Large and small EV have been isolated from RPMI8226 and OPM2 cells by sequential ultracentrifugation at 20,000 g (20K) and 110,000 g (110K), and the expression of the two NOTCH2 forms was separately assessed by western blot analyses using specific antibodies for NOTCH2 and NOTCH2-IC; TSG101 was used as controls for vesicle protein extracts. **C)** EV-mediated cell-to-cell transfer of NOTCH2: the donor HEK293 cell line was forced to express HA-tagged NOTCH2 carried by pCDNA3.1 or the corresponding empty vector (negative control); EV secreted by donor cells were collected by ultracentrifugation and used to treat receiving HEK293 cells for 24 h. Cell and EV protein extracts were analyzed by western blot using a specific primary antibody anti-HA. α-Tubulin and TSG101 were used to normalize cellular and vesicular protein extract loading, respectively. NOTCH2-IC identified by re-hybridazation of the same membrane with anti-NOTCH-IC (see Fig.S3) is indicated by an asterisk.

Fig.4: Molecular effects of NOTCH2 modulation on MM-EV. A) Western blot analysis confirms the KD efficacy on NOTCH2-TM levels in HMCL and the produced MM-EV. α-Tubulin and TSG101 have been used as loading controls for cell and vesicle protein extracts, respectively. **B)** NTA on MM-EV^{SCR} and MM-EV^{N2KD} from HMCL does not show significant changes in concentration and size; D50=size point below which 50% of the EV are contained. Data are expressed as mean value ± SEM of at least four experiments (RPMI8226 n=4; OPM2 n=6). Statistics by two-tail T-test did not show any significant difference. **C)** MM-derived EV activate NOTCH signaling in receiving cells: a NOTCH reporter assay was carried out on HeLa cells stimulated with MM-EV^{SCR} and MM-EV^{N2KD} from HMCL (EV derived from OPM2 cells), or control fresh medium (w/o EV). Luciferase activity is expressed as the ratio between Nano/Firefly luciferase luminescence units. Data are expressed as mean value ± SE of at 4 experiments. Statistics by ANOVA and Tukey post-test: *=p<0.05. **D)** Activation of NOTCH signaling in the trunk of *Tg(T2KTp1bglob:hmgb1-mCherry)* zebrafish embryos (zf) 4 h after the injection of MM-EV^{SCR} and MM-EV^{N2KD} (EV derived from RPMI8226 cells), or control fresh medium (w/o EV). Representative pictures of each condition are reported on the left (20x and 60x magnification, the upper and the lower respectively); a graph on the right represents the mean value +/- SEM of the corrected total fluorescence (CTF) measured in caudal hematopoietic tissue (CHT). In particular four *in vivo* experiments involved zf embryos injected with negative control (n=20) or MM-EV^{SCR} (n=27) and MM-EV^{N2KD} (n=27). Statistics by ANOVA and Tukey post-test excluding outliers identified through the ROUT method (Q=1%): *=p<0.05; ****=p<0.0001.

Fig.5: NOTCH2 contributes to the protumorigenic communication of MM-EV toward osteoclasts and endothelial cells. A) The effect of MM-EV^{SCR} and MM-EV^{N2KD} collected from the osteoclastogenic cell line RPMI8226. The Raw264.7 cell line was treated with or without the osteoclastogenic RANKL (30 ng/ml), MM-EV or control fresh medium (w/o EV). After 7 days TRAP positive multinucleated cells (≥3 nuclei) were enumerated (TRAP positive multinucleated cells were indicated by an arrow). Representative images are shown for each condition on the left (4x magnification); a graph on the right represents the mean value of the absolute number of TRAP+ multinucleated cells +/- SEM. Statistical analysis by a one-way ANOVA with Tukey post-test; *= p < 0.05. **B)** Tumor angiogenesis induced by MM-EV^{SCR} and MM-EV^{N2KD}**.** Tube formation assay performed for 13h with HPAEC laid on a matrigel-coated support stimulated with MM-EV^{SCR} and MM-EV^{N2KD} collected from RPMI8226 and OPM2 cells or control fresh medium (w/o EV). The graphs show the mean values of areas and nodes (branch points) enumerated in four quadrant of the well +/- SEM. Statistical analysis was performed by ANOVA and Tukey post-test; *= p <0.05, **= p <0.01. Representative images are shown below for each condition (4x magnification).

Fig.6: γ-Secretase blockage of NOTCH2 activation inhibits the effect of MM-EV on osteoclastogenesis and angiogenesis. **A)** Experimental rationale. MM-EV derived NOTCH2 may increase NOTCH signaling activation on target cells (OCL progenitors and EC) that may be blocked by DAPT administration. **B)** Raw267.4 cells induced to differentiate into OCLs in the presence of 30 ng/ml

RANKL were treated with MM-EV collected from the osteoclastogenic cell line RPMI8226 or the control fresh medium (w/o EV) and in the presence or absence of DAPT to inhibit NOTCH signaling activation. For each condition a negative control cultured in the absence of RANKL has been carried out. After 7 days TRAP+ multinucleated cells (≥3 nuclei) were enumerated. The graph shows the mean values of TRAP+ multinucleated cells obtained in the different conditions for RANKL treated cells. Given the large number of conditions, to make the graph simpler and easier to understand, each value has been subtracted of the respective control without RANKL (+/- SEM). Statistical analysis was performed by a one-way ANOVA with Tukey post-test; *=p < 0.05;***= p < 0.001. **C)** Tube formation assay on HPAEC was performed for 13 h with MM-EV collected from RPMI8226 and OPM2 cells or control fresh medium (w/o EV) in the presence or the absence of DAPT. The graphs show the mean values of areas and nodes enumerated in four quadrant of the well +/- SEM. Statistical analysis was performed by ANOVA and Tukey post-test; *= p <0.05, **= p <0.01. **D)** Tube formation assay on HPAEC treated for 13 h with EV collected from the BM of MGUS patients or MM patients in the presence or the absence of DAPT. The graphs show the mean values of areas and nodes enumerated in four quadrant of the well (+/- SEM). Statistical analysis was performed by ANOVA and Tukey post-test; **= p <0.01, ****= p <0.001. The characteristics and number of MM patients are reported in table S1.

Fig.1

A

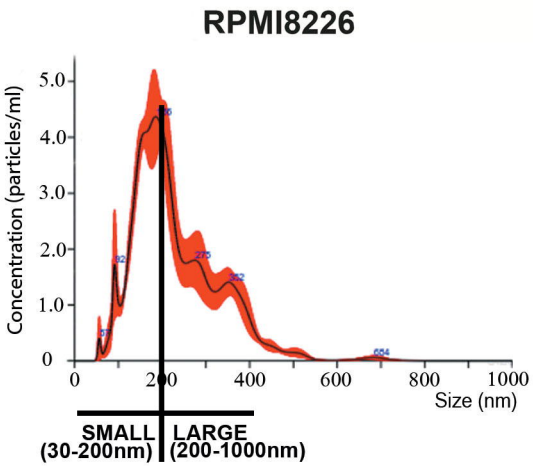
RPMI8226
Concentration (particles/ml)
5.0
4.0
3.0
2.0
1.0
0
0
200
400
600
800
1000
Size (nm)
SMALL
(30-200nm)
LARGE
(200-1000nm)

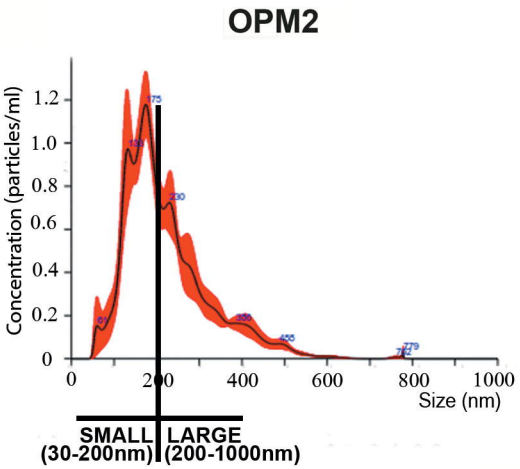
OPM2
Concentration (particles/ml)
1.2
1.0
0.8
0.6
0.4
0.2
0
0
200
400
600
800
1000
Size (nm)
SMALL
(30-200nm)
LARGE
(200-1000nm)

B

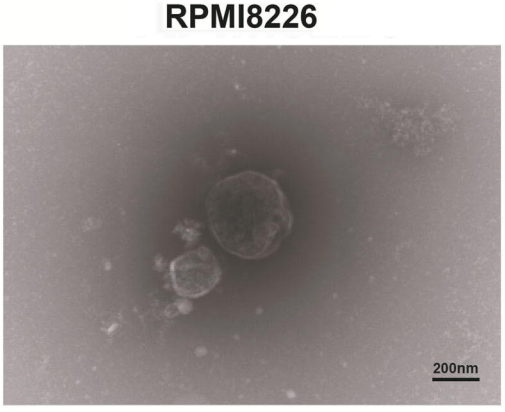
RPMI8226
200nm

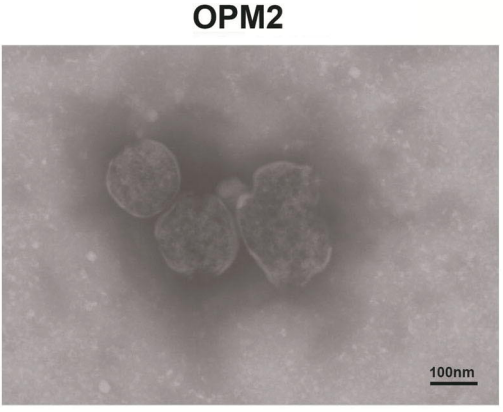
OPM2
100nm

Fig.2

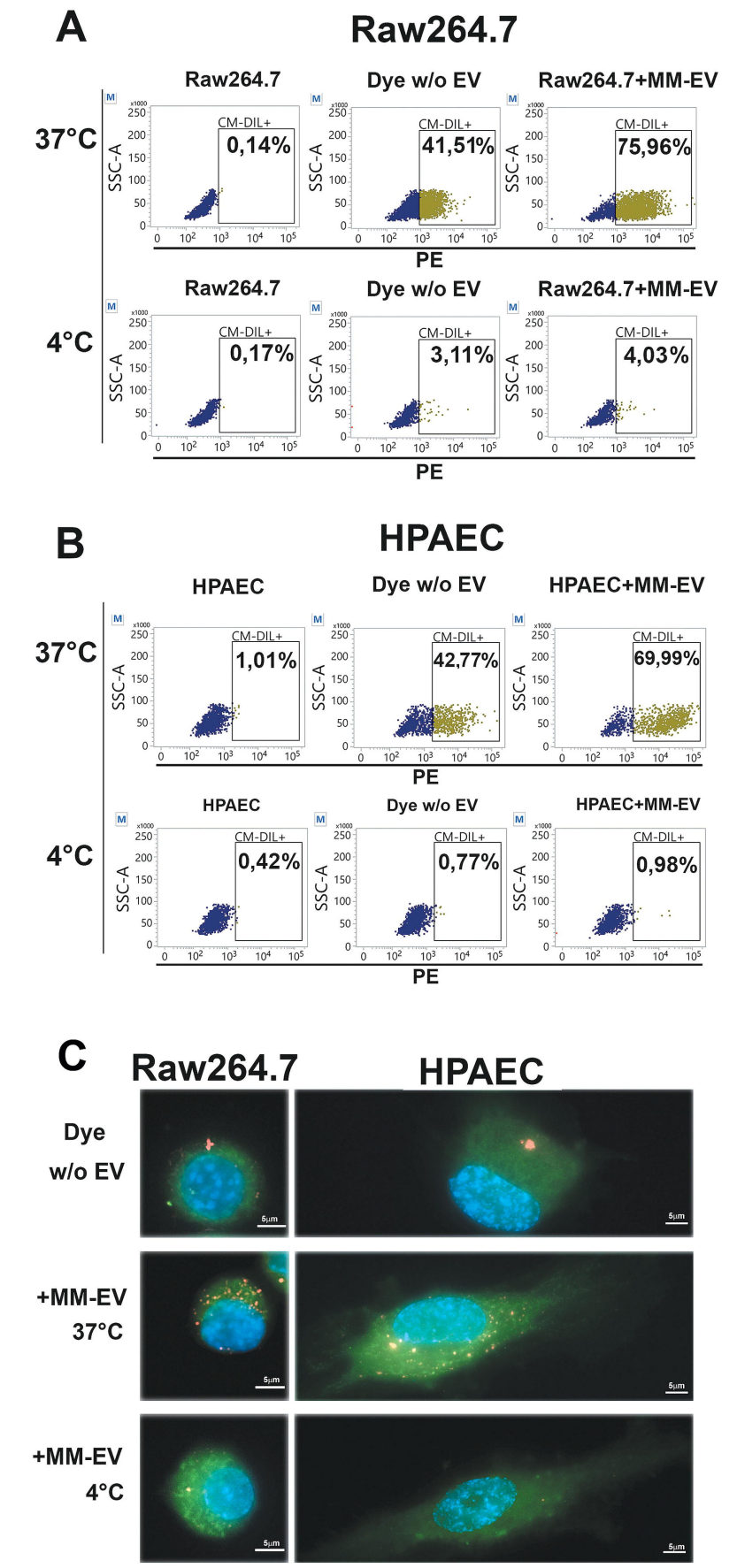
A
Raw264.7
Raw264.7
Dye w/o EV
Raw264.7+MM-EV
37°C
4°C
CM-DIL+
0,14%
41,51%
75,96%
0,17%
3,11%
4,03%
SSC-A
PE
B
HPAEC
HPAEC
Dye w/o EV
HPAEC+MM-EV
37°C
4°C
1,01%
42,77%
69,99%
0,42%
0,77%
0,98%
C
Raw264.7
HPAEC
Dye
w/o EV
+MM-EV
37°C
+MM-EV
4°C
5µm

Fig.3

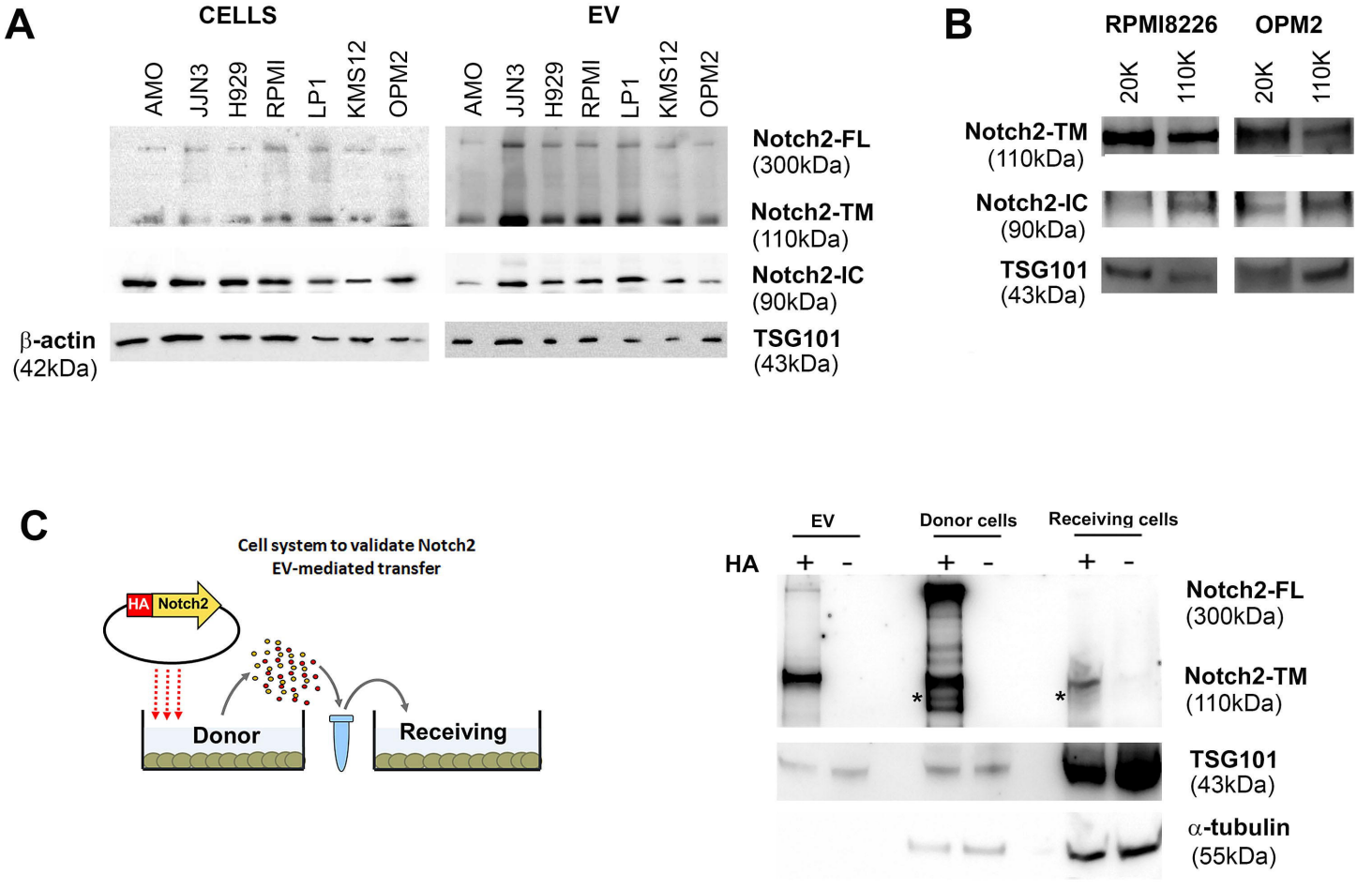
A
CELLS
EV
AMO
JJN3
H929
RPMI
LP1
KMS12
OPM2
Notch2-FL
(300kDa)
Notch2-TM
(110kDa)
Notch2-IC
(90kDa)
TSG101
(43kDa)
β-actin
(42kDa)
B
RPMI8226
OPM2
20K
110K
Notch2-TM
(110kDa)
Notch2-IC
(90kDa)
TSG101
(43kDa)
C
Cell system to validate Notch2
EV-mediated transfer
HA
Notch2
Donor
Receiving
EV
Donor cells
Receiving cells
HA
+
-
Notch2-FL
(300kDa)
Notch2-TM
(110kDa)
TSG101
(43kDa)
α-tubulin
(55kDa)

Fig.4

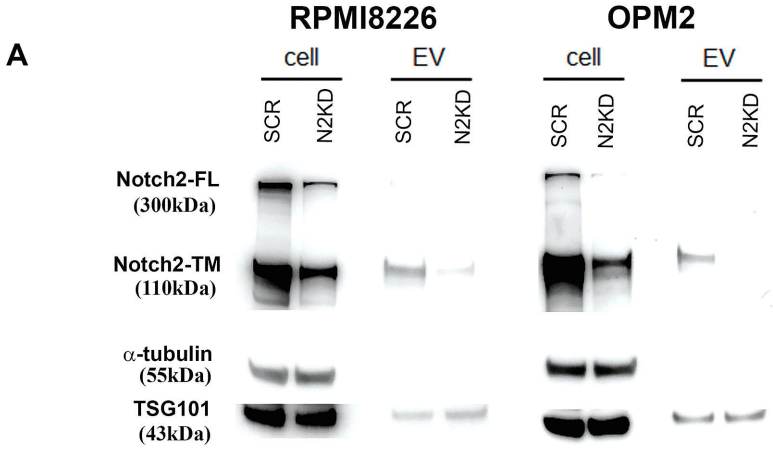
A
RPMI8226
OPM2
cell
EV
cell
EV
SCR
N2KD
SCR
N2KD
SCR
N2KD
SCR
N2KD
Notch2-FL
(300kDa)
Notch2-TM
(110kDa)
α-tubulin
(55kDa)
TSG101
(43kDa)

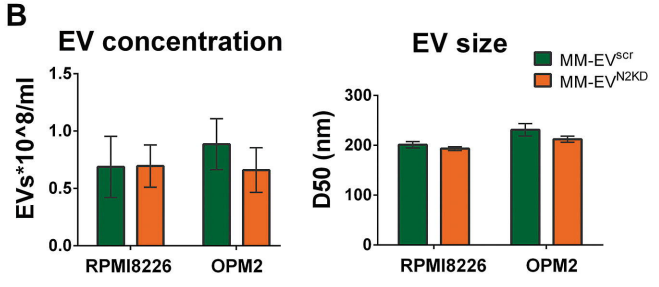
B
EV concentration
EVs*10^8/ml
1.5
1.0
0.5
0.0
RPMI8226
OPM2
EV size
MM-EV^scr
MM-EV^N2KD
D50 (nm)
300
200
100
0
RPMI8226
OPM2

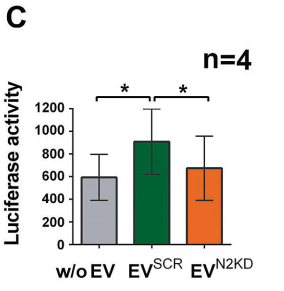
C
n=4
Luciferase activity
1200
1000
800
600
400
200
0
*
*
w/o EV
EV^SCR
EV^N2KD

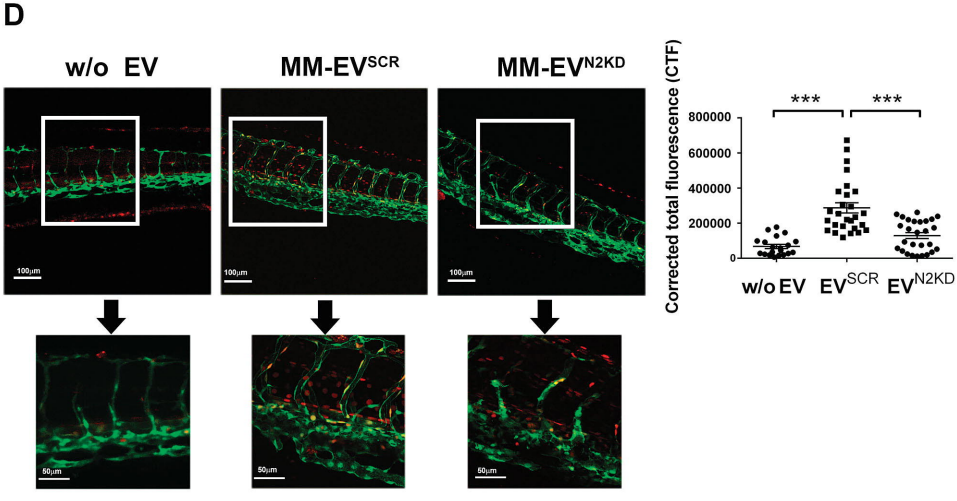
D
w/o EV
MM-EV^SCR
MM-EV^N2KD
100μm
50μm
Corrected total fluorescence (CTF)
800000
600000
400000
200000
0
***
***
w/o EV
EV^SCR
EV^N2KD

Fig.5

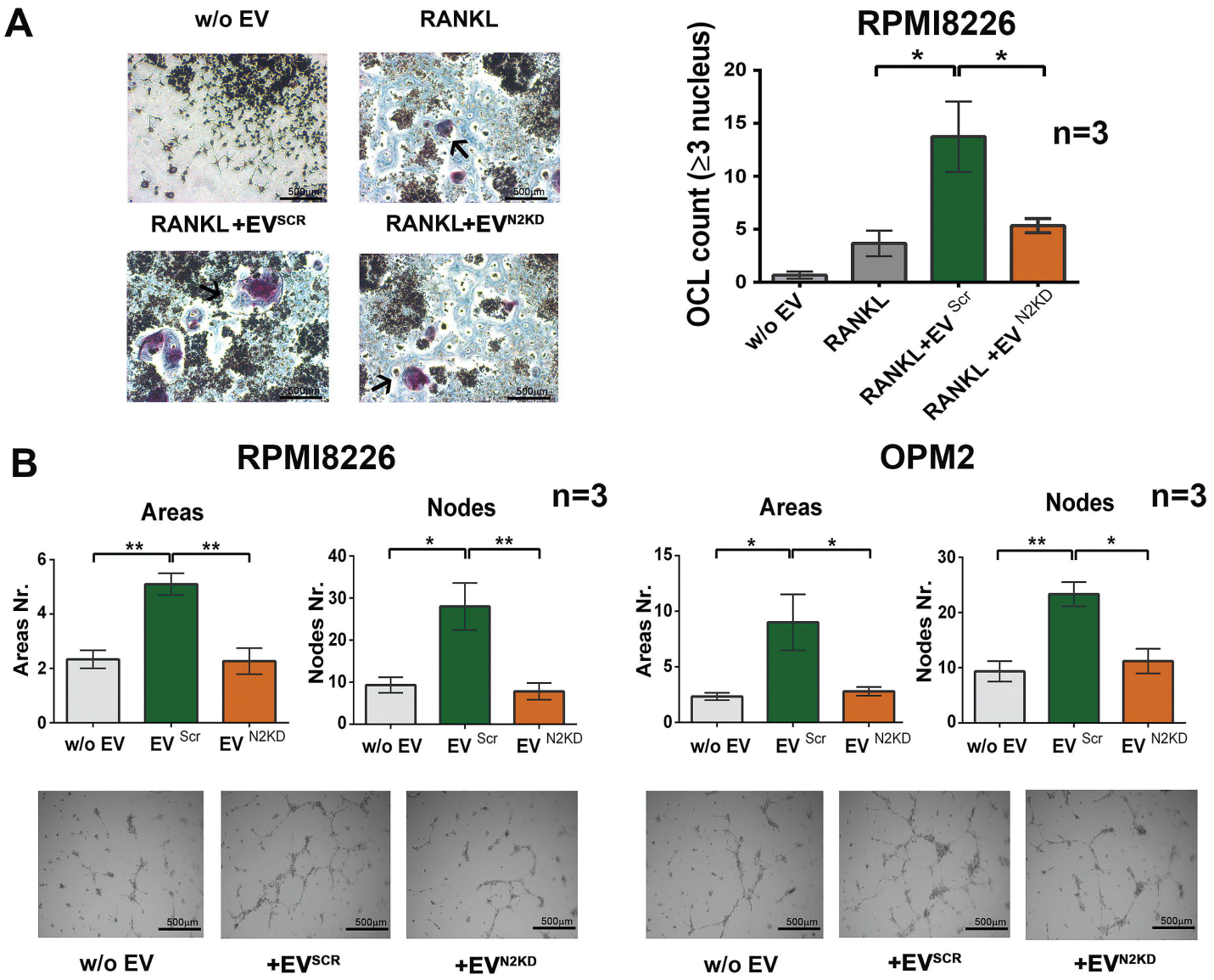
A
w/o EV
RANKL
RANKL+EVSCR
RANKL+EVN2KD
500µm
RPMI8226
OCL count (≥3 nucleus)
n=3
w/o EV
RANKL
RANKL+EV Scr
RANKL +EV N2KD
B
RPMI8226
OPM2
Areas
Nodes
Areas Nr.
Nodes Nr.
n=3
w/o EV
EV Scr
EV N2KD
+EVSCR
+EVN2KD

Fig.6

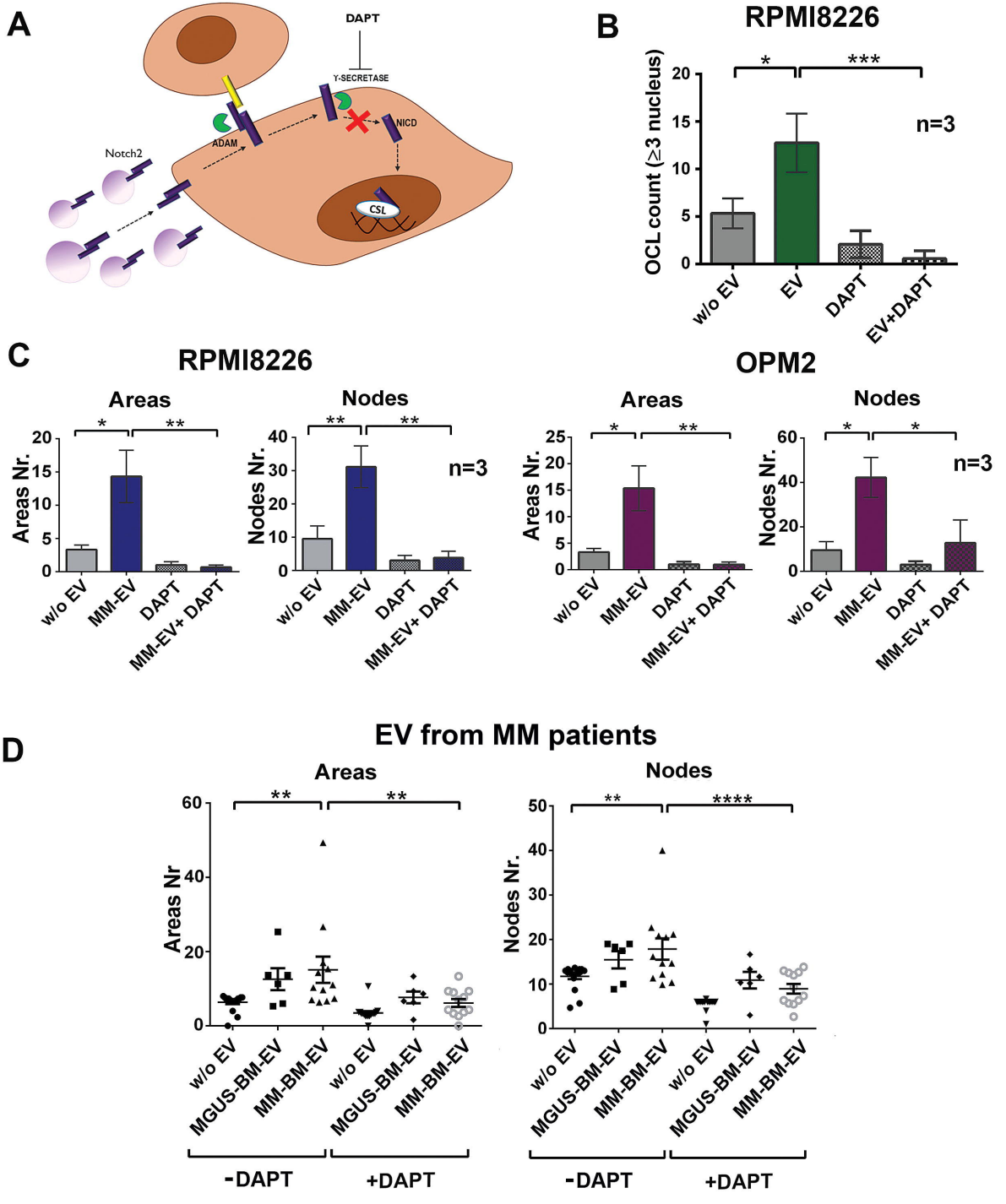
A
DAPT
Y-SECRETASE
ADAM
NICD
Notch2
CSL
B
RPMI8226
OCL count (≥3 nucleus)
n=3
w/o EV
EV
DAPT
EV+DAPT
C
RPMI8226
OPM2
Areas
Nodes
Areas Nr.
Nodes Nr.
n=3
w/o EV
MM-EV
DAPT
MM-EV+ DAPT
D
EV from MM patients
Areas
Nodes
Areas Nr
Nodes Nr.
w/o EV
MGUS-BM-EV
MM-BM-EV
-DAPT
+DAPT

Extracellular vesicles mediate the communication between multiple myeloma and bone marrow microenvironment in a NOTCH dependent way

Domenica Giannandrea, Natalia Platonova, Michela Colombo, Mara Mazzola, Valentina Citro, Raffaella Adami, Filippo Maltoni, Silvia Ancona, Vincenza Dolo, Ilaria Giusti, Andrea Basile, Anna Pistocchi, Laura Cantone, Valentina Bollati, Lavinia Casati, Elisabetta Calzavara, Mauro Turrini, Elena Lesma, Raffaella Chiaramonte.

SUPPLEMENTARY INFORMATION

INVENTORY

Supplemental Information contains the Supplemental Data (six figures, one table and two supplemental videos) and Supplemental experimental Procedures.

Supplemental Data:

Figure S1 is related to Fig. 2

Figures S2 and S3 are related to Fig.3

Figure S4 and S5 are related to Fig.4

Figure S6 is related to Fig. 5

Table S1 is related to Fig. 6

Supplemental videos (video 1 and 2) are related to Fig. 2

.

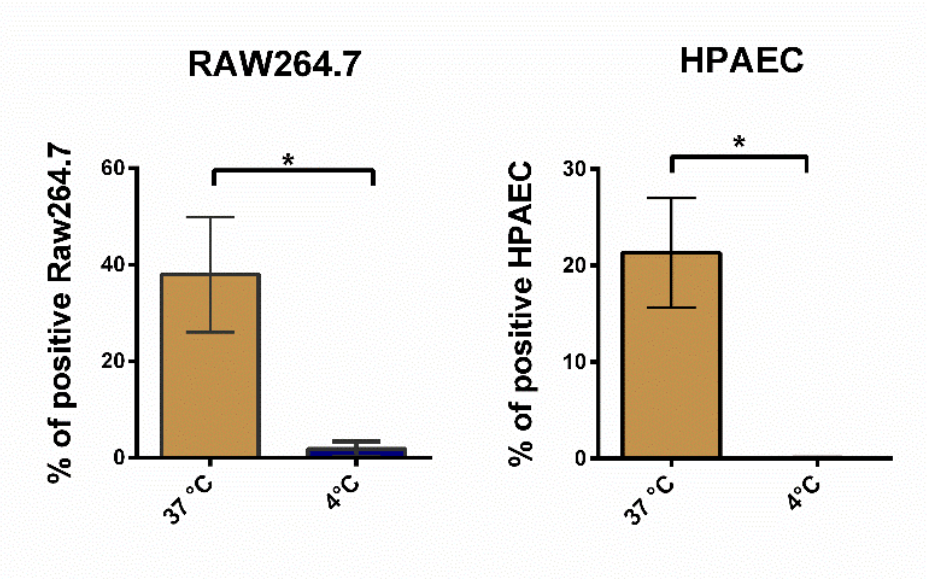

Fig. S1. **Flow cytometry analysis of EV uptake in osteoclast progenitors and endothelial cells.** Flow cytometry analysis mean percentage values of CM-DIL positive Raw264.7 cells and HPAEC after treatment with CM-DIL labeled RPMI8226-EV at 37°C and 4°C. The data are normalized on the negative control. Data are presented as mean values of three independent experiments. Statistics are by two-tailed Student t-test: *=$p<0.05$.

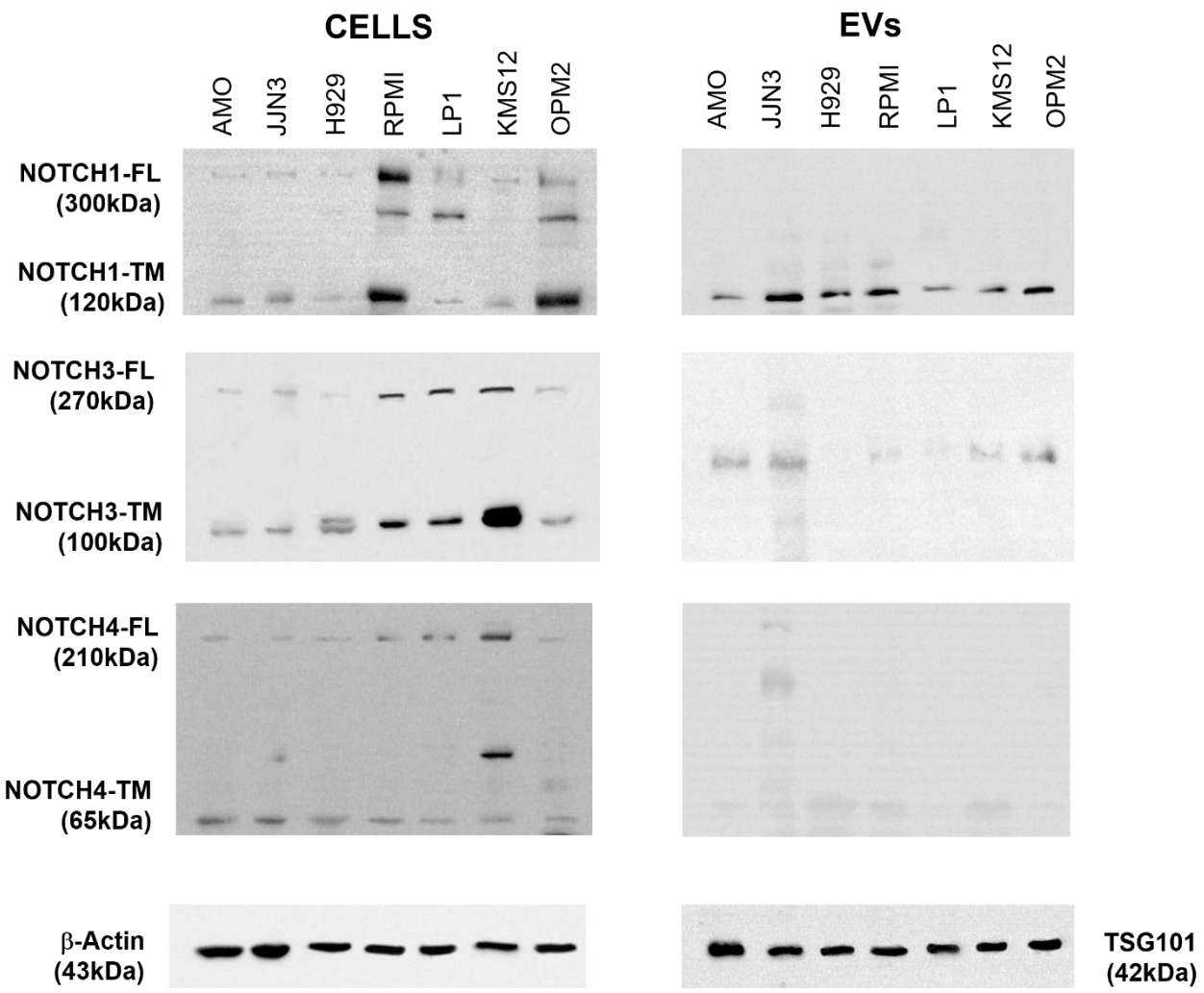

Fig.S2. Western blot analysis for NOTCH1, NOTCH3 and NOTCH4 in HMCL: Western blot analysis for NOTCH1, NOTCH3 and NOTCH4 expressed in 7 different HMCL and the respective shed EV. β-Actin and TSG101 have been used as loading controls for cells and vesicle protein extracts, respectively.

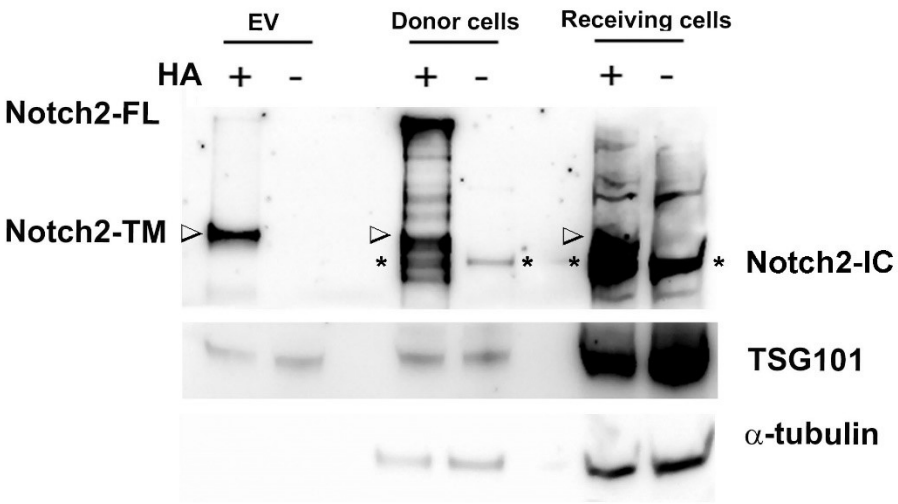

Fig.S3. EV-mediated cell-to-cell transfer of NOTCH2-IC: the membrane of Western blot for NOTCH2-HA shown in Fig.2C was re-hybridized with anti-NOTCH2-IC antibody. Although this antibody cannot distinguish between endogenous NOTCH2-IC and NOTCH2-IC tagged with HA, the signals detected in the negative controls of donor and receiving cells allowed us to identify which among the bands in Fig.2C revealed with the anti-HA antibody represents the NOTCH2-IC form. The identified bands of NOTCH2-IC have been reported here (as well as in Fig.2C) with asterisks. For a better comprehension the bands of NOTCH2-TM revealed by the previous hybridization of this membrane with the anti-HA antibody have been marked with a triangle. By comparing the images in Fig.2C and Fig.S3, we could clarify that in this cell system, NOTCH2-IC is not carried by EV cargo, although it is present in donor cells. On the other side a small amount of transferred NOTCH2-HA seems to be activated when reaching the receiving cells.

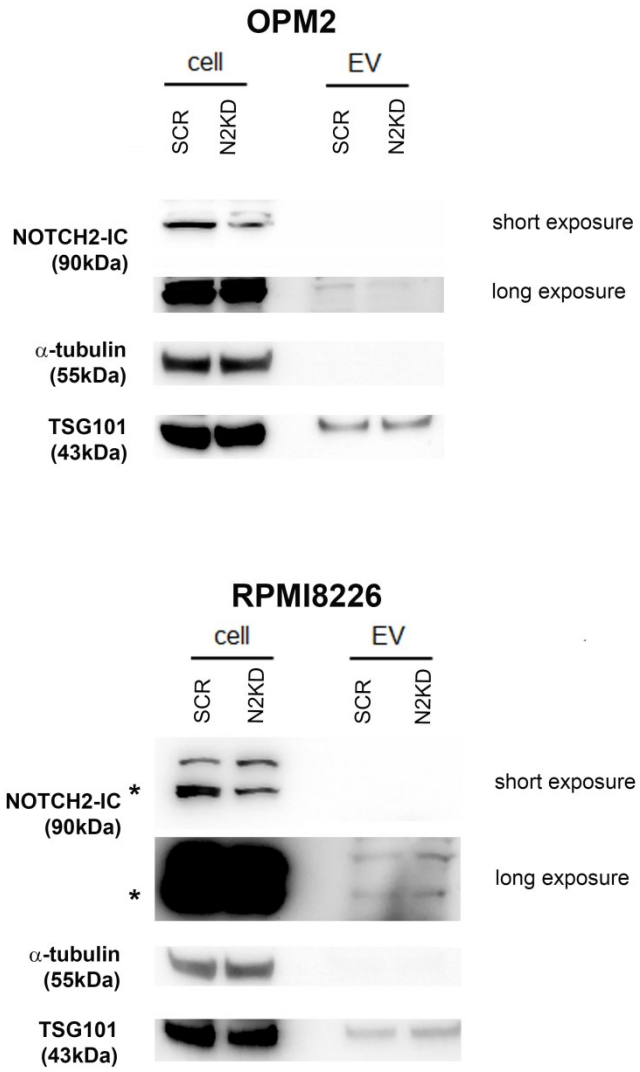

Fig.S4 Immunoblot analysis of NOTCH2-IC on HMCL knockdown for NOTCH2. Western blotting revealed a decrease in NOTCH2-IC in both cell types upon NOTCH2 lentiviral silencing and a clear reduction in OPM2-derived MM-EV, while no significant differences are detectable in RPMI8226-derived EV. EV protein extract loading was half as cell extracts, therefore, to detect NOTCH2-IC in cell lysate a short exposure is shown, while a long exposure is shown to detect it in EV extracts. An asterisk indicates the NOTCH2-IC band in protein extracts from RPMI8226 cells and EV to distinguish it from the aspecific band above. α–Tubulin and TSG101 have been used as loading controls for cell and vesicle protein extracts, respectively.

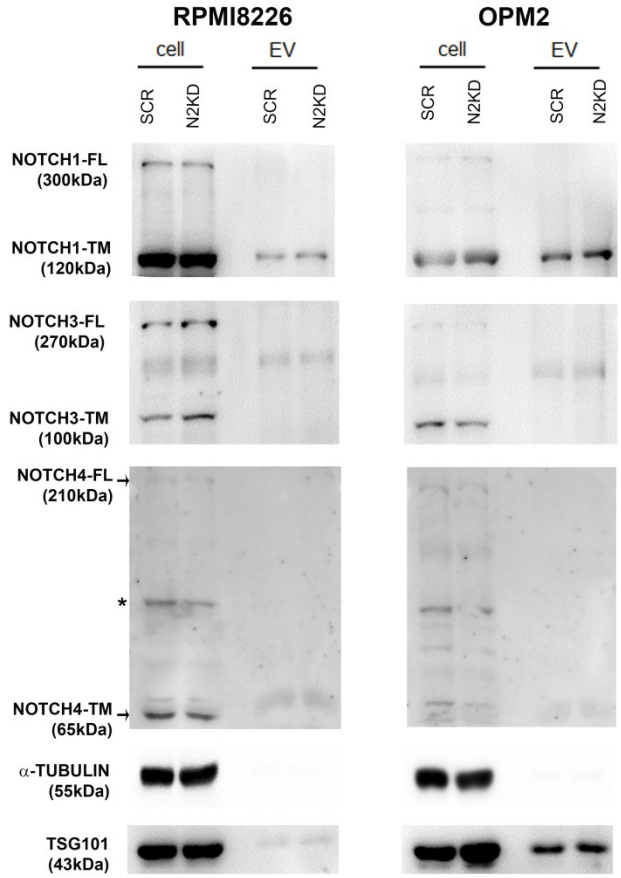

Fig.S5 Immunoblot analysis of NOTCH1, NOTCH3 and NOTCH4 on HMCL knockdown for NOTCH2. Western blotting revealed no differences in the protein levels of NOTCH1, NOTCH3 and NOTCH4 in HMCL and the shed MM-EV upon NOTCH2 lentiviral silencing. Equal amounts of total protein for each sample were loaded. α–Tubulin and TSG101 have been used as loading controls for cell and vesicle protein extracts, respectively. The arrow indicates NOTCH4-FL. Asterisk shows non-specific band detected by the antibody.

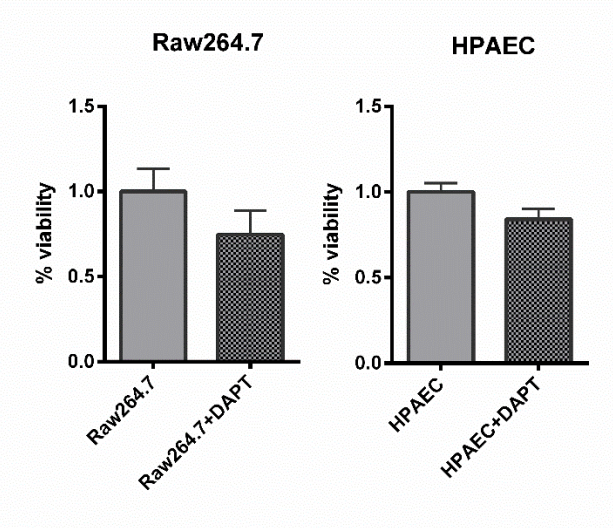

Fig. S6 Viability assay of OCL and EC upon DAPT treatment. MTT assay on Raw264.7 cells and HPAEC treated with DAPT 50μM. The data were expressed as percentage of mean values +/- SEM of three independent experiments. The statistical analysis carried out with one-tailed t-test did not detect any statistically significant difference.

	All patients		**MGUS**		**MM**	
Patients, no. (M/F)	18	(10/8)	6	(3/3)	12	(7/5)
Median age, y (IQR)	74	(16)	74	(16)	77	(15)
Median BM PC, % (IQR)	37.5	(57.0)	8.0	(3.0)	57.5	(30)
Median M-protein, g/dl (IQR)	2.33	(2.99)	0.90	(0.78)	3.57	(2.07)
Median U-protein, g/24h (IQR)	0.35	(0.43)	0.17	(0.25)	0.50	(0.98)
Median sFLC, mg/L (IQR)	397.5	(1083.1)	132.2	(318.2)	605.0	(1244.1)
Median B2-MG, mg/L (IQR)	3.77	(3.80)	2.30	(1.40)	4.30	(3.56)
Median calcemia, mg/dl (IQR)	9.5	(0.8)	9.6	(0.3)	9.0	(1.0)
Median WBC, x 10^9/L (IQR)	5.00	(2.78)	4.75	(2.78)	5.21	(2.42)
Median Hb, g/dl (IQR)	12.2	(4.2)	13.1	(1.3)	10.3	(3.8)
Median PLT, x 10^9/L (IQR)	195	(75)	188	(46)	207	(123)

Table S1. Clinical characteristics at presentation of patients. B2-MG: B2-microglobulin; BM PC: bone marrow plasma cells; Hb: hemoglobin; IQR: interquartile range; M-protein: seric monoclonal protein; MGUS: monoclonal gammopathy of undetermined significance; MM: multiple myeloma; PLT: platelets; sFLC: involved seric free light chains; U-protein: urinary monoclonal protein; WBC: white blood cells

Supplemental videos 1 and 2 (provided as separate files). Fluorescence microscopy analysis of EV uptake in bone marrow cells. Video stack analysis of the EV internalization in Raw264.7 cells (video 1) and HPAEC cells (video 2) treated with CM-DIL positive MM-EV performed by z-stack imaging.

Supplemental experimental procedures

Cells and treatments

The human MM cell lines (HMCL), AMO1 (ACC-538), JJN3 (ACC-541), KMS12 (ACC-551), LP1 (ACC- 41), OPM2 (ACC-50) were purchased from DSMZ collection of microorganisms whereas RPMI8226 (ATCC® CCL-155) and H929 (ATCC® CRL-906) were purchased from cell cultures and the American Type Culture Collection. HMCL were cultured in RPMI1640 (Euroclone, Italy) supplemented with 10% Fetal bovine serum (FBS) (Euroclone, Italy), 100U/ml penicillin/streptomycin (Microgem, Italy) and 2mM L-glutamine (Microgem, Italy).

The primary human pulmonary artery endothelial cells (HPAEC, ATCC® PCS-100-022) were purchased from the American Type Culture Collection and cultured in Vascular Basal medium (ATCC® PCS-100-030TM) supplemented with Endothelial cells Growth Kit-VEGF (ATCC® PCS-100-041TM) following the manufacturer instruction.
Human embryonic kidney 293 cells, HEK293T (ATCC® CRL-157), HeLa cells (ATCC® CCL-2™), and the murine pre-osteoclasts Raw264.7 (ATCC® TIB-71) were purchased from the American Type Culture Collection and cultured in Dulbecco's modified Eagle's medium (DMEM; Euroclone, Italy) with 10% FBS, 100U/ml penicillin/streptomycin and 2mM L-glutamine.
Recombinant human Receptor Activator of Nuclear Factor κ B (RANKL) (Immunotools, Germany) was resuspended in phosphate buffered saline (PBS) supplemented with 0,1% w/v Bovine Serum Albumin (BSA) and used at 30ng/ml for 7 days as reported. N-[N-(3,5-difluorophenacetyl-L-alanyl)]-S-phenylglycine *t*-Butyl ester (DAPT; Merck, Germany), solubilized in dimethylsulphoxide (DMSO), was used at a final concentration of 50μM.

Isolation and treatment with of extracellular vesicles

MM cell lines were seeded at a density of $3x10^5$ cells/ ml in RPMI1640 with 10% EV-depleted FBS previously obtained with 16 h ultracentrifugation at 110,000 g at 4°C. After 48 h, cell debris and aggregates were removed by centrifugation at increasing speeds 1,000 g, 2,000 g, and 3,000 g for

15 min at 4°C and EV were collected by 75 min ultracentrifugation at 110,000 g at 4°C using a Himac CP100NX ultracentrifuge (Himac, Japan)
The obtained pellet was resuspended in 0,1µm filtered PBS for characterization of size and concentration by Nanoparticles Tracking Analysis (NTA) or for the analysis by transition electronic microscopy (TEM). For western blot analyses EV were resuspended in Radioimmunoprecipitation assay (RIPA) buffer and quantified using a Bradford assay (Himedia, Italy). For functional assays, EV were resuspended in serum-free medium RPMI1640. For osteoclastogenesis and angiogenesis, we used an amount of EV isolated from one equivalent volume of the conditioned medium of producing HMCL, or half volume in the case of EV purified by BM aspirates, while for NOTCH reporter assay *in vitro* EV were concentrated 40 times. The ultracentrifuged fresh culture medium + 10% FBS previously depleted of bovine EV was used as negative control.
To isolate different EV subpopulations, firstly CM was ultracentrifuged 30 min at 10,000 g at 4°C to remove cell debris and apoptotic bodies and then the supernatant was subsequentially ultracentrifuged 75 min at 20,000 g to obtain large EV and after at 110,000 g for 75 min at 4 °C to collect small vesicles. The obtained pellets were resuspended in RIPA buffer for western blot analysis.

Nanoparticle tracking analysis

Size and concentration of EV were determined by NanoSight NS300 system (Malvern Panalytical Ltd, Malvern, UK). A camera level of 12 and five 30-s recordings were used for acquisition of each sample. Data were analyzed with NTA software (Malvern Panalytical Ltd.).

Transmission electron microscopy

EV resuspended in PBS were adsorbed into 300-mesh carbon-coated copper grids for 5 min, room temperature, then fixed in 2% glutaraldehyde in PBS for 10 min and briefly rinsed in Milli-Q water. After negative staining with 2% phosphotungstic acid, brought to pH 7,0 with NaOH, grids were examined with a Microscope Zeiss STEM GEMINI 500. All materials are from Electron Microscopy Sciences, Hatfield, PA, USA.

***In vitro* internalization assays of extracellular vesicles**

EV were isolated from the 48 h conditioned medium (CM) of RPMI8226 cells as reported above, stained with the 1µg/ml cell-tracker CM-DIL (Invitrogen, USA) following manufacturer's instructions and washed with 0,1µm filtered PBS by 75 min ultracentrifugation to remove the non-binding dye. An ultracentrifugation tube containing only PBS and the dye was used as a negative control. 15µg EV stained with the dye or negative control were used to treat a monolayer of Raw264.7 cells or HPAEC for 4 h at 37°C or 4°C. The uptake efficiency was assessed by flow cytometry and fluorescence microscopy.

For quantitative assessment of EV uptake, Raw264.7 cells and HPAEC were seeded at the density of 1,5 x 10^5 cells/ ml in 48-well (Euroclone S.p.A, Italy) with 250μl of DMEM supplemented with 10% FBS or with Vascular Basal medium supplemented with Endothelial cells Growth Kit-VEGF respectively. After 24 h, cells were treated with CM-DIL dye labelled-EV or with negative control at 37°C and 4°C. After 4h, the medium was removed, and the cells were washed with PBS and treated with trypsin. For flow cytometry, cells resuspended in PBS were analyzed in PE channel to assess the CM-DIL positive cells by using the FACS Verse flow cytometry (BD Biosciences, Italy).

For microscopy analysis, Raw264.7 cells or HPAEC cells were stained with 5μM CFSE (Biolegend, Italy) following manufacturer's instructions and seeded 3,5 x 10^4 cells/ml in 24 chamber slides in 500 μl of the appropriated complete medium. After treatment with EV, the slides were washed with PBS and fixed with PFA 2% for 15 min. Fixed cells were washed with PBS and stained with 4′,6-diamidino-2-phenylindole (DAPI). The analysis was performed with a DM-IRE 2 Leica microscope equipped with a Retiga Electro CCD camera and Micro-Manager software. Images were acquired in z-stack scan mode with a HCX PL APO 63x objective, by applying the same acquisition setting, excitation intensity, acquisition time, step size.

Western Blot

Whole cells or EV extracts were prepared in RIPA lysis buffer with the proteases and phosphatases inhibitors cocktail (Sigma Aldrich, Italy). Protein samples (5-40μg) were run on 4-12% gradient SDS gel electrophoresis (Genscript, USA), transferred onto a nitrocellulose membrane (Hybond-ECL, Amersham Bioscience, Italy), and blocked with 5% nonfat milk in TBS-T (20 mM Tris-Cl, pH 7.5, 150 mM NaCl, 0,05% Tween 20). Membranes were incubated overnight at 4°C with anti-NOTCH1 (D1E11) antibody (1:1000 dilution, Cell Signaling Technology, USA), anti-NOTCH2 (D76A6) antibody (1:1000 dilution, Cell Signaling Technology, USA), anti-NOTCH2 cleaved from Val1697 (SAB4502022) antibody (1:1000 dilution, Sigma-Aldrich, St. Louis, MI, USA); anti-NOTCH3 (D11B8) antibody (1:1000 dilution, Cell Signaling Technology, USA), anti-NOTCH4 (STJ90070) antibody (1:1000 St John's Laboratory Ltd. , London, England, United Kingdom);anti-HA (C29F4) antibody (1:1000 dilution, Cell Signaling Technology, USA), anti-TSG101 (ab125011) antibody (1:500 dilution, AbCam, Cambridge, UK), α-tubulin (sc-12462) antibody (1:1000 dilution, Santa Cruz Biotechnology, USA), β-actin (1:1000, Sigma Aldrich, Italy) followed by incubation with the appropriated HRP-conjugated species-specific secondary antibody (Promega, Italy). Chemiluminescence was detected by the Western Bright ECL HRP substrate (Advansta Inc., USA) or by Super Signal™ West Femto Maximum Sensitivity Substrate (Thermo Fisher Scientific, Italy) and using the Alliance HD 6 western blot imaging system (Uvitec, UK).

HEK293-cell based system to track NOTCH2 EV-mediated transfer from donor to receiving cells

For HEK293 cells transfection the cDNA NOTCH2-HA was subcloned from pcDNA5/FRT NOTCH2-HA provided by Groot AJ [1] into pcDNA3.1 2,5 × 10^6 cells HEK293 cells were transfected in 100mm plate with pcDNA3.1-NOTCH2-HA (N2-HA) plasmid or mock pcDNA3.1 (as a control) plasmid using TurboFect transfection reagent (ThermoScientific) according to the manufacturer's protocol. The medium was replaced after 16 h incubation at 37°C with DMEM 10% FBS and, to obtain EV carrying NOTCH2-HA or control EV, the donor cells were cultured 24 h in DMEM with 10% EV depleted-FBS. EV were purified by 75 min ultracentrifugation at 110,000 g, 4°C. The isolated NOTCH2-HA or control EV were added to the medium of receiving HEK293 cells for 24 h. Cell extracts of donor or receiving cells, and EV extracts were analyzed by western blot using an anti-HA primary antibody and subsequently re-hybridized.

Lentivirus production and transduction of stable HMCLs with shRNAs

Lentiviral vectors pTRIPZ (Horizon Discovery, United Kingdom) expressing scrambled (SCR) or NOTCH2 shRNAs were transfected with Trans-Lentiviral shRNA Packaging mix (Horizon Discovery, United Kingdom) into HEK293 cells using calcium phosphate reagent according to the manufacturer's instructions. Briefly, 5,5x10^6 cells seeded 24 h prior of transfection were transfected with 42µg pTRIPZ shRNA vector and 30µl Trans-Lentiviral packaging mix using the calcium phosphate reagent. After 16 h calcium phosphate-containing medium was removed from cells and replaced with DMEM supplemented 5% FBS. The viral supernatants were collected at 24 and 48 h post-transfection, filtered, and concentrated using 20% sucrose cushion ultracentrifugation for 4 h at 40,000 g at 4°C to obtain the lentiviral particles.

RPMI8226 and OPM2 cell lines were transduced with the lentiviral particles in presence 20ng/ml IL6 (Peprotech, USA) and 20ng/ml IGF1 (Peprotech, USA) for 48 h by exposing the cells twice to fresh viral supernatant. After 48 h, the infected RPMI8226 and OPM2 cells were selected for stable expression with puromycin at a minimum concentration, as determined by a killing curve, 1µg/mL and 0,5µg/ml, respectively. After 7-10 days under puromycin selection the knockdown efficiency was monitored in transduced cells using 1µg/mL doxycycline to induce TurboRFP and shRNA expression. RFP expression was detected in PE channel by flow cytometry using FACS Verse (BD Biosciences, Italy) whereas the efficiency of NOTCH2 knockdown was evaluated by western blot analysis of cell lysate. Single cell colonies were obtained from a stable SCR and NOTCH2 shRNAs cell pools by limiting dilution. Colonies with maximum NOTCH2 knockdown efficiency were chosen for the further experiments. To produce EV from $HMCL^{SCR}$ and $HMCL^{N2KD}$, cell lines were maintained for 7 days with Doxycycline 1µg/ml, changing the medium every 2 days; for the last 48 h cells were cultured in complete medium depleted of bovine EV as reported above.

NOTCH reporter assay

HeLa cells were transiently transfected with 240ng of the NOTCH responsive element pNL2.1-6xCSL [2] and with 240ng of the thymidine kinase promoter-driven Firefly luciferase expressing vector (RL-TK pGL4.54) used as a normalizer for the transfection. After 16h, HeLa cells were seeded 12,5 x 10^3 cell/well in a 96-well and treated with 100μl of MM-EV resuspended in complete RPMI1640 or the corresponding negative control (see above). After 24 h, luciferase activity was measured using Nano-Glo® Dual-Luciferase® Reporter (NanoDLR™, N1620, Promega, Italy) and the Glowmax instrument (Promega, Italy).

***In vivo* experiments**

Transgenic zebrafish (*Danio rerio*) embryos obtained by crossing *Tg(T2KTp1bglob:hmgb1-mCherry)* with *Tg(fli1a:EGFP)* were obtained from the Wilson lab, University College London, London, United Kingdom. Zebrafish embryos were raised and maintained under standard conditions and national guidelines (Italian decree 4th March 2014, n.26).

Embryos were collected by natural spawning, staged according to Kimmel and colleagues [3] and raised at 28°C in fish water (Instant Ocean, 0,1% Methylene Blue) in Petri dishes, according to established techniques. We express the embryonic ages in hours post fertilization (hpf) and days post fertilization (dpf). After 24 hpf, to prevent pigmentation 0,003% 1-phenyl-2-thiourea was added to the fish water.

Before EV microinjections, zebrafish embryos were washed, dechorionated for 5 to 10 min with 1mg/ml pronase 48 hpf and anaesthetized with 0,016% tricaine (Ethyl 3-aminobenzoate methanesulfonate salt; Sigma-Aldrich). For each embryo, 10nl of EV produced by 6000 RPMI8226 cells were resuspended in PBS and injected into the duct of Cuvier with a manual microinjector (Eppendorf, Hamburg, Germany) using glass microinjection needles. Following injections, embryos were kept at 28 °C for 30 min and at 32 °C for the duration of the experiments.

To evaluate MM-EV mediated NOTCH activation in zebrafish embryos, the efficiency of MM-EV uptake was evaluated 4 hours post injection (hpi) by fluorescence microscopy using the Leica DM 5500B microscope equipped with the DC480 camera. We measured fluorescence intensity in the trunk region, specifically in the caudal hematopoietic tissue (CHT) area on photomicrographs with ImageJ software. Images were processed using the Adobe Photoshop program.

Representative images were acquired in confocal microscopy using Leica TCS SP2 AOBS equipped with 405 diodes, 488 Ar/ArKr and 543 HeNe lasers and analyzed by Leica Confocal Software (Leica Microsystems, Wetzlar, Germany). 20x images were acquired in xyz scan mode with a 20x objective, by applying comparable arrangement parameters: PMT gain/offset voltages, step size, scan speed, frame, and line average. Sequential scan mode between frames was applied to reduce the fluorophore cross talking between 543 and 488 emission and obtain all scans at the same current z position. 60x images were acquired with the same parameters using a 20x objective with additional 3x electronic zoom.

Osteoclast differentiation assay

Raw264.7 cells were seeded in a 48-well plate in 250µl of RPMI1640 medium supplemented with 10% FBS at a density of $1,25\times10^4$ cells/ well with or without 30ng/ml RANKL and treated every 48h with RPMI8226 cell derived-EV or negative control. For experiment with DAPT, cells were treated with MM-EV or the control medium with the drug or the vehicle.
After 7 days, Raw264.7 cells were fixed on the culture plates with citrate-acetone solution and stained for tartrate resistant acid phosphatase (TRAP kit, Sigma-Aldrich). Osteoclasts were identified and enumerated under light microscopy as TRAP positive cells with ≥3 nuclei.
Representative pictures of TRAP positive osteoclasts were acquired with Olympus U-CMAD3 phase-contrast microscope equipped with a Zeiss Axiocam ICc1 camera at 4x magnification.

Angiogenesis assay

For tube formation assay, Growth Factor reduced Matrigel (Corning, NY, USA) was dispensed in a 96-well plate, 50µL/well, and incubated for 30 min at 37°C. For each well, 8×10^3 HPAEC were seeded and cultured for 13 h in 100µl of serum-free RPMI1640 with MM-EV or the control medium. For experiment with DAPT, cells were treated with MM-EV or the control medium with the drug or the vehicle. Pictures of the tube-like structures were acquired with the EVOS-inverted microscope (Euroclone, Italy) at 4x magnification. Numbers of areas and nodes were analyzed using the ImageJ software.

Cell viability assay

Raw264.7 and HPAEC were seeded at the same concentration used for the functional assays with EV and treated with 50µM of DAPT for 13 h or 7 days, respectively. After the appropriate experimental time 0,6mg/ml 3-(4,5-dimethylthiazole-2-yl)-2,5-diphenyl tetrazolium bromide (MTT; Sigma) was added to each well for 3 h at 37°C. Formazan crystals were dissolved in 0.01N HCL isopropanol. Specific absorbance was read at 570 nm with subtraction of background at 690 nm. The percentage of cell viability is expressed as: (absorbance treated wells / absorbance of control wells) x 100%.

***Ex vivo* experiments with EV from patients' BM aspirates**

EV were isolated from the BM aspirates of monoclonal gammopathy of undetermined significance (MGUS) (MGUS-BM-EV) and MM patients (MM-BM-EV). The Institutional Review Board of Insubria Italy approved the design of this study (approval n. 1/2018). Written informed consent was obtained in accordance with the Declaration of Helsinki. Clinical information of patients is reported in table S1.

The blood samples were collected at the diagnosis in tubes containing disodium EDTA and processed to obtain plasma through centrifugation at 250 × g for 20 minutes at RT. To isolate EV, the obtained plasma sample was diluted 1:3 with cold PBS and centrifuged three times at increasing speed and ultracentrifuged as reported above. For functional assays, the obtained EV were resuspended in serum-free RPMI1640 in the same original volume and used at a 0,5x final concentration. The functional assays were performed as reported above.

Statistical analyses

Statistical analyses were performed using Student t-test to compare the mean values of two data sets and ANOVA with Tukey post-test for multi-comparison analyses.
The sample minimum size for each *in vivo* experiment on zebrafish embryo was determined based on a priori power analysis for a one-way ANOVA with an alpha level of 0,05 aimed to have power of 0,95, performed on data from a pilot study with 5 embryos for each condition (G-power 3.2 software)[4]. Each *in vivo* experiment involved at least 16 embryos divided in 4 groups. The final analysis was performed by one-way ANOVA with Tukey post-test on data from 4 independent experiments, excluding outliers identified through the ROUT method (Q=1%) [5].

References

1. Groot AJ, Habets R, Yahyanejad S, et al. Regulated proteolysis of NOTCH2 and NOTCH3 receptors by ADAM10 and presenilins. Mol Cell Biol. 2014;34(15):2822-32.

2. Colombo M, Garavelli S, Mazzola M, et al. Multiple myeloma exploits Jagged1 and Jagged2 to promote intrinsic and bone marrow-dependent drug resistance. Haematologica. 2020;105(7):1925-1936.

3. Kimmel CB, Ballard WW, Kimmel SR, Ullmann B,Schilling TF. Stages of embryonic development of the zebrafish. Dev Dyn. 1995;203(3):253-310.

4. Faul F, Erdfelder E, Lang AG,Buchner A. G*Power 3: a flexible statistical power analysis program for the social, behavioral, and biomedical sciences. Behav Res Methods. 2007;39(2):175-91.

5. Motulsky HJ,Brown RE. Detecting outliers when fitting data with nonlinear regression – a new method based on robust nonlinear regression and the false discovery rate. BMC Bioinformatics. 2006;7(1):123.